

Institut für Angewandte Physik
der Universität Bonn

Wegelerstraße 8
53115 Bonn

Three-Level Physics of a Single Atom Coupled to a High Finesse Cavity

von
Martin Eckstein

Diplomarbeit in Physik

angefertigt im
Institut für Angewandte Physik

vorgelegt der
Mathematisch-Naturwissenschaftlichen Fakultät
der Rheinischen Friedrich-Wilhelms-Universität
Bonn
im April 2010

Referent: Prof. Dr. D. Meschede
Korreferent: Priv.-Doz. Dr. E. Soergel

Contents

1	Introduction	3
2	The Experiment	5
2.1	Magneto-Optical Trap and Dipole Trap	5
2.2	Optical Conveyor Belt and the High Finesse Cavity	5
2.3	Raman Setup	6
2.3.1	The Optical Phase Lock Loop	7
2.3.2	Implementation into the Setup	9
3	Stimulated Raman Transitions of a Few Atoms	11
3.1	Theory of Stimulated Raman Transitions	11
3.2	Push-Out Technique	16
3.3	Spectra	16
3.3.1	Setup	16
3.3.2	Spectra of Zeeman-Sublevels	17
3.3.3	Optical Pumping	18
3.4	Raman-Rabi Oscillations	20
3.5	Conclusion	23
4	Performance of the Optical Phase Lock Loop	25
4.1	Characterization of the Phase Noise	25
4.1.1	Beat Signal	25
4.1.2	Quadrature	26
4.2	Theoretical Analysis of the Lock	30
4.2.1	Control Theory	32
4.2.2	Elements of the Optical Phase Lock Loop	33
4.3	Measurement of the Frequency Modulation Response of the System	33
4.3.1	Influence of the Thermal Response of the Laser Diode to Frequency Modulation	35
4.3.2	Performance of the Phase Lead-Lag Filter	36
4.3.3	The Finite Loop Delay	36
4.4	Conclusion	36
5	Electromagnetically Induced Transparency of a Single Atom	39
5.1	EIT	39

5.2	Measurement	42
5.3	Interpretation of the Measurement	44
5.3.1	Semi-classical Approach	44
5.3.2	The Cavity	47
5.4	Conclusion	51
6	Summary and Outlook	53
	Bibliography	54

1 Introduction

The perpetual interaction between light and the countless atoms and molecules surrounding us is forming the colors and shapes of the images we see with our eyes. Our experiment replicates this interaction in the most fundamental but also demonstrative way: A single caesium atom interacts with a single photon.

On this fundamental level the quantized structure of our world becomes visible and furthermore can be utilized to store and process information with the quanta. The fundamental building block of information theory, the bit, has an analogon in the quantum world the **qubit**. Factoring algorithms using the qubits can be a lot faster [1], possibly making classical cryptography protocols for data communication insecure. At the same time the qubit provides the cure for this problem, since information encoded, for example in light quanta, is inherently secure against eavesdropping. Impressive experimental realizations of both problems have been achieved in the recent past in [2] and [3], however an economic use of these techniques still lies in the far future.

In our experiment the qubit is found in the two stable hyperfine ground states of the caesium atom. To make it experimentally accessible, the atoms are laser cooled to the μK regime and then located inside a ultra high finesse optical resonator. The coherent interaction between the resonator mode and the atom is enhanced by the high reflectivity of the mirrors, and the qubit state can non-destructively be measured via the cavity transmission. This is an important step and was recently realized [4].

In order to use the system for quantum information processing, the so called entanglement between qubits is necessary. In the experiment this could be achieved by placing two atoms side by side into the resonator and applying a deterministical control over the interaction via the cavity mode. This control would be realized by an additional laser that illuminates the atoms from the side of the cavity. The coupling of an atom to the cavity mode can then be switched on and off via a stimulated Raman transition between the two qubit states of the atom. A Raman transition connects the qubit states via a third intermediate state of the atom with the help of two off-resonant light beams. During the transition the radiative state is almost unpopulated and therefore incoherent scattering, which would destroy the qubit coherence, can be avoided [5]. In order to drive the Raman transition two lasers operating with a frequency difference fixed to the energy difference of the two qubit states are needed. In our setup a so called optical phase lock loop (OPLL) provides this possibility. This lock was built by Karsten Schörner[6] but not yet successfully used in combination with the main experiment.

In this thesis I present two steps on the road to the entanglement of the two atoms. First I was able to improve the lock stability. The Raman setup was then connected with

1 Introduction

the main experiment. As a first test the stimulated Raman transitions were induced on atoms that were trapped in a dipole trap. The functionality of the lock and the successful implementation into the main experiment could be demonstrated, and are described in the first and second chapter of the thesis. In this connection the performance of the lock was the object of closer investigations. I implemented an additional analysis tool to measure the quality of the lock more reliable and as well did more investigations on the limiting factors of the performance of the lock. These results are presented in the third chapter.

After the successful test of the Raman setup it was possible to combine it with the cavity. As the main experimental result it was possible to demonstrate electromagnetically induced transparency with a single atom. The two ground states are again connected via a third radiative state, but this time the two light fields are on resonance with the atomic resonance frequencies. EIT is understood as an interference effect in the excitation paths of the atoms that lead to a suppression of the absorption of the light. The effect was extensively studied in the last two decades on large atomic ensembles, since the modified dispersive response can lead to such interesting effects such as slow light [7–9] or even the complete stop of light [10]. For single atom a similar effect (STIRAP) was exploited to store the information a single photon qubit carries into the atomic qubit [11]. While absorption can be suppressed due to the EIT effect in our system, the nonlinear optical response of the atomic medium could be enhanced to create an effective photon-photon interaction, which forms the basis for a quantum gate with photons as flying qubits [12].

2 The Experiment

In order to provide the background for the measurements presented in the thesis I will shortly summarize the current existing experimental setup. I will refer to previous Diplom theses and PhD theses where possible and go more into detail for the changes of the setup that were done during my Diplom studies time. A conceptual drawing of the setup is given in 2.1.

2.1 Magneto-Optical Trap and Dipole Trap

The start point of all experiments is a magneto-optical-trap (MOT) that catches and cools caesium atoms from the background gas of a ultra high vacuum. The cycling transition for laser cooling is formed between the upper hyper-fine splitted ground state $F = 4$ and the highest hyperfine state $F' = 5$ of the $6^2P_{3/2}$ manifold (852nm). The energy-level scheme for caesium is shown in figure 2.2. A repumping laser is needed to counteract off-resonant scattering from $F = 4$ to $F = 3$. The number of atoms inside the MOT can be counted via the fluorescence light. By changing the MOT from a low (30 G/cm) to a high magnetic gradient (300 G/cm), the capture range of the MOT can be reduced, and no additional atoms are loaded into the trap. By adjusting the loading time it is possible to determine the number of atoms loaded into the MOT, down to a few atoms. The atoms are then transferred into a far-off resonant dipole trap (FORT) operating at 1030 nm. The dipole trap is formed by two counter-propagating beams forming a standing wave pattern with an intensity periodicity of $\lambda/2$. By the attractive dipole force the atoms will be dragged to the high intensity regions and feel a harmonic potential with a trap depth of around 1 mK, resulting in a typical temperature of 200 μ K for the atoms. For the parameters of our setup the atoms have a trap frequency of 410 kHz in the axial direction of the dipole trap and a trap frequency of 3.3 kHz in radial direction [13].

2.2 Optical Conveyor Belt and the High Finesse Cavity

By slightly detuning the frequency of one of the dipole trap arms, it is possible to spatially move the potential wells of the trap. If the frequency detuning is done slowly enough, the atoms will stay in their potential wells and are dragged along the axis of the dipole trap. A detailed description of this technique can be found in [14]. Exploiting this technique the atoms can be moved with sub-micrometer precision between the two mirrors of an ultra high finesse cavity with $\mathcal{F} = 1.1 \cdot 10^6$. The cavity has a length of 158 μ m resulting in a free spectral range of $\frac{c}{2L} \approx 950$ THz. The high finesse requires an elaborate locking scheme

2 The Experiment

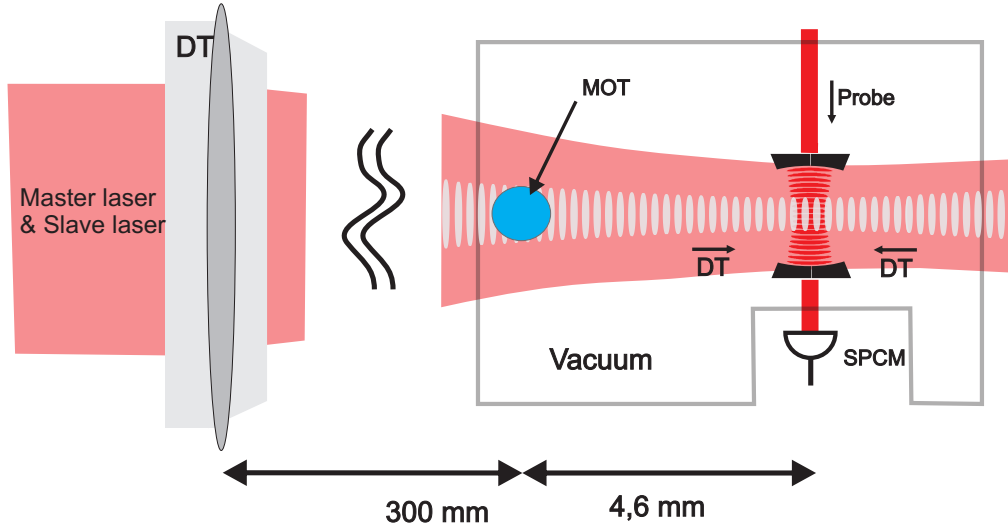


Figure 2.1: Single caesium atoms are caught in a MOT from the background gas of an ultra high vacuum. The atoms are then loaded into standing wave far-off resonant dipole trap (DT). By detuning the frequency of one of the dipole trap arms the atoms can be spatially moved along the dipole trap axis. Via this "optical conveyor belt" the atoms can be positioned between the mirrors of an ultra-high-finesse cavity. The cavity is weakly probed and the transmission through the cavity is detected by a single photon counting module (SPCM). The beams of the master and the slave laser of the new Raman setup are aligned to the dipole trap axis illuminating MOT and cavity at once. In contrast to the dipole trap they are not forming a standing wave pattern, since they are shone in only from one side of the vacuum cell. For a more detailed description of the cavity geometry and the beam geometry of the beams see figure 3.3.

that is able to stabilize the cavity length to a few femtometers with respect to the wavelength of the light that is probing the cavity. The cavity transmission is detected via a single photon counting module (SPCM)[14].

2.3 Raman Setup

Since the main goal of this thesis is to drive lambda-type two-photon processes it is essential to have an experimental setup that can stabilize the frequency difference between two lasers to the hyperfine ground state splitting of cesium ($\Delta_{\text{HFS}} = 9.192631770\text{GHz}$). For this purpose an optical phase lock loop was built that is able to phase lock two laser to a desired frequency offset. The details of the lock built by Karsten Schörner are described in [6]. However I will now briefly summarize the functioning of the lock.

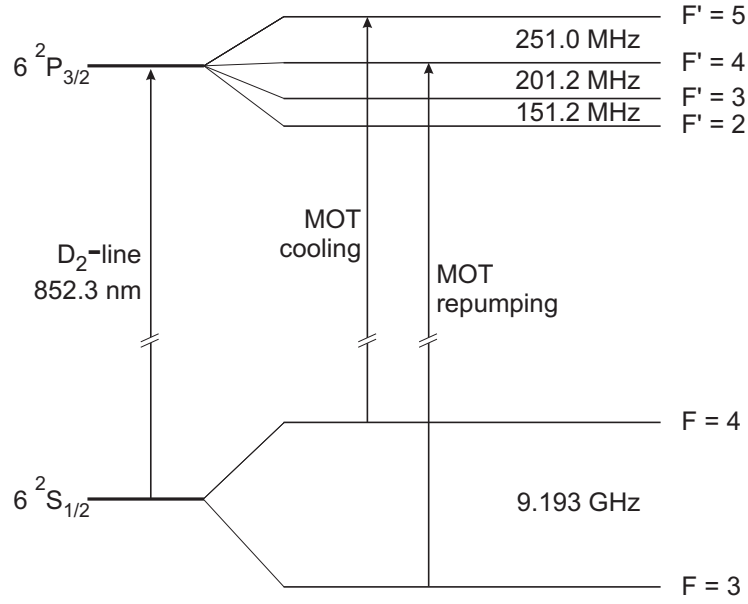


Figure 2.2: The cycling transition for the MOT can be found in caesium between the upper hyperfine state $F = 4$ and the excited state $F' = 5$ of the D₂-line. Off-resonant scattering from $F = 4$ to $F = 3$ will be counteracted by a repumpig laser that is resonant with the $F = 3$ to $F' = 4$ transition.

2.3.1 The Optical Phase Lock Loop

An optical phase lock loop (OPLL) is a negative feedback system that stabilizes the optical phase of a so called slave laser ϕ_S to a reference optical phase given by another laser, the so called master laser ϕ_M . Ideally the slave laser will track the optical phase of the master laser at any given point of time. The setup for the lock is shown in figure 2.3. All laser are diode lasers in Littrow configuration. The basic idea behind the lock is to superpose the two laser on a fast photodiode and use the interference between the two beams as a possible source for an error signal that tunes the frequency of the slave laser. When both beams have the same linear polarization the intensity detected by the fast photo diode reads

$$\begin{aligned}
 I_{PD} &\propto |E_M \cos(\omega_M t + \phi_M) + E_S \cos(\omega_S t + \phi_S)|^2 \\
 &= \cos^2(\omega_M t + \phi_M) |E_M|^2 + \cos^2(\omega_S t + \phi_S) |E_S|^2 \\
 &\quad + 2E_M E_S \cos(\omega_M t + \phi_M) \cdot \cos(\omega_S t + \phi_S) \\
 &= E_M E_S \cos((\omega_M - \omega_S)t + \phi_M - \phi_S) + f(\omega_M + \omega_S, \omega_M, \omega_S),
 \end{aligned} \tag{2.1}$$

where f is a function summarizing fast oscillating terms. The fast photo diode in the setup can only detect frequency modulations in the range 8.2 GHz to 9.8 GHz and will provide an AC-signal. Faster modulations will be suppressed and not amplified, hence the laser frequencies and the sum frequency are suppressed. The frequency difference contribution,

2 The Experiment

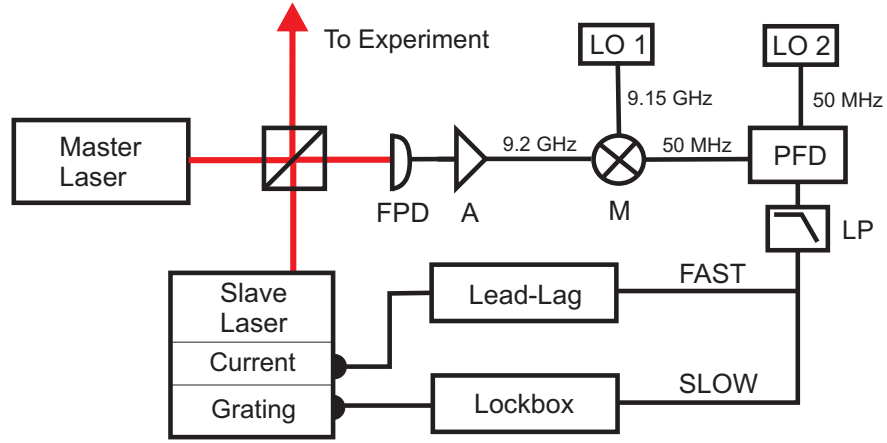


Figure 2.3: Master and slaver laser are superposed on a fast photo diode (FPD). The beat signal, resulting from the frequency offset between the laser, is amplified (A) and then mixed (M) with a local oscillator source (LO 1). The down converted beat signal can be processed by a phase frequency detector (PFD). Together with a low pass (LP) the detector provides an error signal proportional to the phase difference between beat signal and a second local oscillator source (LO 2). The error signal is split and used as the source of a two-path feedback loop. A slow feedback modulates the grating inside the diode laser via a lock box. A fast feedback is filtered by a lead-lag filter and directly modulates the laser current.

from now on called beat signal, however, can be amplified with a low noise amplifier. The idea behind to lock is to mix the beat signal with a local oscillator source. The mixing is again a multiplication yielding a sum and difference contribution, where again the sum contribution is suppressed. One gets then the following error signal

$$\text{Error}(t) \propto \cos((\omega_M - \omega_S - \omega_{LO})t + \phi_M - \phi_S - \phi_{LO}). \quad (2.2)$$

The phase of the LO will be set to $\phi_{LO} = \pi/2$, which can be done without losing any information. When the local oscillator frequency equals the frequency difference between the two laser, the error signal is proportional to the sine of optical phase difference between the lasers.

$$\text{Error}(t) = \sin(\phi_M(t) - \phi_S(t)) \quad (2.3)$$

In the actual setup the phase detection is replaced by an digital phase frequency detector (PFD) with a successive low pass to average the output of the detector in order to use it as the error signal. In order to use the PFD the beat signal has to be down converted to smaller frequency, since PFD only works for frequencies up to 200 MHz. The down conversion is done by mixing the beat signal with a local oscillator source (LO1), running with frequency difference in the range of 50 MHz to the beat signal. In principle the

digital element works the same as an analog mixer, it compares the beat signal with a local oscillator source (LO2), but has the advantage that it gives a linear response for phase deviations from $-\pi$ to π (not the sine like a normal mixer) and can switch into a frequency detection modus for larger deviations than π , i.e. the output of the detector will stay at maximum amplitude when the phase deviations exceeds the linear response range. By using the output signal of the PFD with the successive low pass as the error signal and by choosing the sum of the local oscillator frequencies (LO1+LO2) it is now possible to adjust the lasers to the exact desired frequency difference. This is done in the following way.

The error signal is split and used as the source for an two-path feedback loop. A slow feedback path controls the grating inside the slave laser, via a PI-controller (lockbox) and a piezo (PZT). This path is slow and therefore can only compensate disturbances with low frequencies up to a few kHz. The advantage is the high gain and the large modulation amplitude of the grating. The capture range of the lock is determined by this feedback path. A fast feedback path is filtered by a so called lead-lag filter and then directly modulates the laser diode current. This feedback loop is much faster in response, up to 2 MHz. The filter is mainly a high pass that is increasing the bandwidth of the lock by lifting the phase of the error signal (see chapter 4 for more details). The fast feedback loop will determine the phase stability of the lock. Detailed information about specifications and functioning of all constituents of the setup can be found in the Diplom thesis of Karsten Schoerner [6]. A more detailed analysis of the lock performance and the limitations of the system will be made in chapter 4.

2.3.2 Implementation into the Setup

I changed some settings of the lock before implementing the OPLL into the main experiment. The old slave laser was replaced by a diode laser with a larger mode hop free range. It is now possible to detune the frequency difference between the lasers by changing the LO 2 frequency in range of around 6 MHz quickly without having the lasers falling out of lock. Also the temperature controllers of both lasers were exchanged and their PID settings adjusted. This results in an improved long time stability of the lock. Without having any exceptional disturbances, the lock is now stable over a complete measurement day. The output of the system is then guided through an AOM in double pass configuration which is able to produce pulses down to $10 \mu\text{s}$. The AOM setup has a suppression of the light of $3.3 \cdot 10^{-6}$. The beams are then guided through a self built polarization maintaining fiber to the main experiment. The fiber assures that any alignment inside the OPLL will not influence the alignment at the main experiment. The right handed circularly polarized beams are then shine in along the direction of the dipole trap illuminating MOT and cavity at the same time. See again figure 2.1.

3 Stimulated Raman Transitions of a Few Atoms

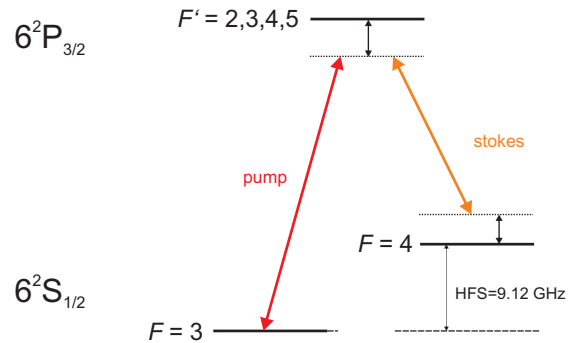
With the Raman setup now connected with the main experiment it is straightforward to test and demonstrate the functioning of the setup in order to use it for its main purpose. Spectroscopic measurements of the hyperfine ground states of caesium via stimulated Raman transitions provide such a possibility, since these type of measurements commonly appear in different varieties in the experiment and their outcome is quite well understood. The measurements are done with on average 10 atoms transferred into the dipole trap at the position of the MOT. As already mentioned the Raman beams are aligned with the direction of the dipole trap, illuminating MOT and cavity at once, in foresight to use the beams also for measurements with atoms inside the cavity. Due to the limited optical access the possible polarization choices for the Raman beams is limited in this case. In the first section of this chapter, the resulting experimental situation arising from this limitation is discussed theoretically. In the second section, first measured spectra of the magnetic substructure of the hyperfine ground states of the atoms are presented. As a subsequent step, measurements of Rabi oscillations between two magnetic substates of optically pumped atoms are presented. The damping of the oscillations could then be compared with the damping of oscillations induced by microwave radiation. Rabi oscillations via microwave transitions were already investigated extensively in the PhD thesis of Stefan Kuhr [15] and thus should serve as an indicator for the performance of the Raman setup.

3.1 Theory of Stimulated Raman Transitions

Stimulated Raman transitions are in general a powerful tool to couple long-lived, non-radiative internal energy states of an atom via a non-populated radiative eigenstate. The long coherence time of the non-radiative states results in a narrow line width of the transition which makes it useful for applications like Raman sideband cooling, where the motional states of atoms trapped in a harmonic potential have to be resolved. The characteristic lambda-type level structure is shown in figure 3.1. The long lived states $|1\rangle$ and $|2\rangle$ correspond in our experiment to the hyperfine ground manifolds of caesium $|6^2S_{1/2}, F = 3\rangle$ and $|6^2S_{1/2}, F = 4\rangle$ respectively, and the radiative state $|3\rangle$ to the $|6^2P_{3/2}\rangle$ manifold. The lower ground state $|1\rangle$ is coupled via a laser, from now on called pump laser, with coupling strength Ω_P to the excited state. The upper ground state $|2\rangle$ is coupled by another laser, called stokes laser, with coupling strength Ω_S to the excited state. Δ is the one-photon detuning and δ the two-photon detuning. For the case of $\delta = 0$, the atom can undergo a two-photon transition via a "virtual" state detuned by Δ from the excited state. By definition, the virtual state is never populated and the system can then be described as

3 Stimulated Raman Transitions of a Few Atoms

Figure 3.1: The long lived ground states $|1\rangle$ and $|2\rangle$ are coupled via a virtual level detuned by Δ from the excited state. Δ is the one-photon detuning. δ is two-photon detuning.



an effective two-level system with a single coupling strength. The coupling strength, an effective flopping frequency for a Rabi oscillation and the contrast of the oscillation is given by [16]

$$\Omega_0 = \frac{\Omega_P \Omega_S}{2\Delta}, \quad \Omega_{\text{eff}} = \sqrt{\Omega_0^2 + \delta^2} \quad \text{and} \quad m = \frac{\Omega_0}{\Omega_{\text{eff}}}, \quad (3.1)$$

respectively. For equal coupling strength the coherent population transfer via the virtual level can be compared to the incoherent population transfer by single photon scattering. The two processes are proportional to

$$\Omega_{\text{eff}} \propto \frac{\Omega^2}{\Delta}, \quad \Gamma_{\text{Scattering}} \propto \frac{\Omega^2}{\Delta^2}. \quad (3.2)$$

By choosing a large detuning Δ it is therefore possible to let the coherent Raman process dominate over the incoherent scattering process.

Different coupling strengths of pump and stokes laser can lead to a so called differential light shift. Light coherently interacting with an atom can shift the resonance frequency of the atomic transition for another beam probing the atom. For the two-photon process one beam sees the induced light shift of the other beam. When both beams shift the resonances with a different magnitude, the two-photon resonance as well is shifted. Given by the difference of the single light shifts, and assuming that the detuning for both beams from the excited state is large and thus approximately the same for both beams, the differential light shift reads

$$\delta_{\text{diff}} = \frac{\Omega_S^2}{4\Delta} - \frac{\Omega_P^2}{4\Delta}. \quad (3.3)$$

However, it has to be noticed that the differential light shift can be compensated by tuning the frequencies of the lasers to the new two-photon resonance. The full contrast in a Rabi oscillation can then again be achieved. For the effective coupling strength this statement translates into

$$\Omega_{\text{eff}} = \sqrt{\Omega_0^2 + (\delta + \delta_{\text{diff}})^2}. \quad (3.4)$$

Influence of the Multi-Level Structure of Caesium

In order to take into account the sub-level structure of caesium, I will follow the approach of summing over all different excitation paths of the atom. Even though the lasers are far detuned from the excited state, it is unknown with which virtual level, each corresponding to an excited state, the laser light will interact. Therefore, the modulus of the sum over the excitation amplitudes has to be taken. This can cause destructive or constructive interference between the excitation pathways. The effective coupling strength of a transition between arbitrary magnetic sub levels of the hyperfine ground states can be calculated and will strongly depend on the polarization of the light. For a proof of this method see [17].

The magnetic substructure of the hyperfine ground states and the hyperfine splitting of the D₂ line is shown in figure 3.2. A single coupling strength connecting one of the magnetic sub level of the $|6^2S_{1/2}\rangle$ manifold with one of the magnetic sub levels of excited state, the $|6^2P_{3/2}\rangle$ manifold, is given by its dipole matrix element. The matrix element gives the strength of the coupling between the electric field and the atomic dipole moment of the corresponding transition. It states

$$\Omega_{F,m \rightarrow F',m'} = \frac{\langle F', m' | \mathbf{d} \cdot \mathbf{E} | F, m \rangle}{\hbar}, \quad (3.5)$$

where the prime indicates the excited state. The matrix element can be calculated using the Wigner-Eckart theorem [18], which separates the matrix element into an atom-specific contribution and a geometrical part arising from the coupling of spin and angular momentum of the atom. The geometrical part is closely related to the Clebsch-Gordan coefficients and can be calculated using 3-j and 6-j symbols. The reduced element will then be

$$\langle F', m' | d \cdot E | F, m \rangle = C(m, m', F, F', I_c, J, J', q) \langle J' = 3/2 || er || J = 1/2 \rangle \quad (3.6)$$

$$\begin{aligned} \text{with } C(m, m', F, F', I_c, J, J') = & (-1)^{2F'+J+I_c+m} \sqrt{(2F'+1)(2F+1)(2J+1)} \\ & \cdot \begin{pmatrix} 1 & F' & F \\ -q & m' & -m \end{pmatrix} \begin{Bmatrix} J & J' & 1 \\ F' & F & I_c \end{Bmatrix} \end{aligned}$$

$$J' = 3/2, \quad J = 1/2, \quad I_c = 7/2 \quad \text{and} \quad q = m' - m = \{+1, -1, 0\}.$$

The remaining dipole matrix element $\langle J' = 3/2 || er || J = 1/2 \rangle$ is related to the lifetime of the excited state. The measured value can be found in [18]. The geometrical part reproduces the well known selection rules for single transitions $\Delta F = 0, \pm 1$ and $\Delta m = 0, \pm 1$ with the exclusion that $\Delta F = m = m' = 0$ at once. Here $\Delta m = m' - m$ is defined like this. From now on transitions with $\{\Delta m = 0, \Delta m = +1, \Delta m = -1\}$ will also be labeled $\{\pi, \sigma^+, \sigma^-\}$. The coupling strength for the stimulated Raman process connecting a magnetic sub level m_3 of $F = 3$ with a sub level m_4 of $F = 4$ can now be calculated from the single dipole matrix elements. The summed coupling strength over all possible

3 Stimulated Raman Transitions of a Few Atoms

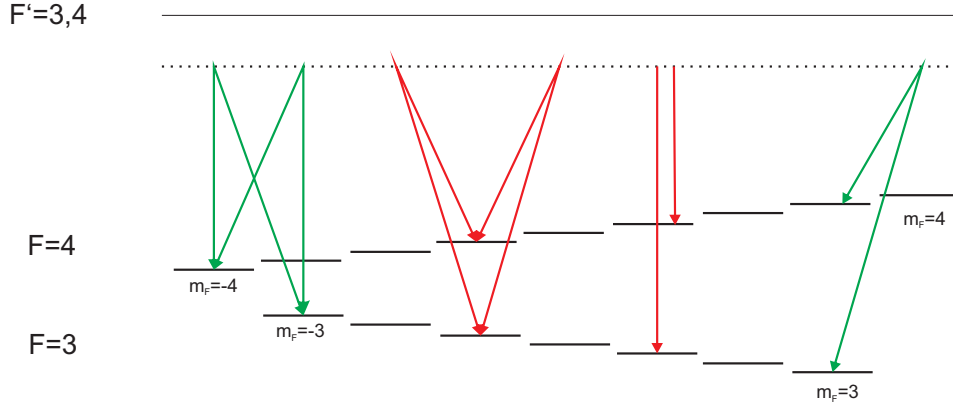


Figure 3.2: The degeneracy of the magnetic substates of the ground hyperfine states is lifted by the Zeeman effect. The Zeeman effect for the substructure of the excited states is not depicted, since it can be neglected, due to the large one-photon detuning. The excited states $F' = 2$ and $F' = 5$ do not participate in the two-photon transitions, due to the selection rules. $\{\pi, \pi\}$ transitions are suppressed by destructive interference between $F' = 3$ and $F' = 4$. $\{\sigma^+, \sigma^+\}$ and $\{\sigma^-, \sigma^-\}$ each interfere constructively, and have the same magnitude but opposite sign. Hence driving both transitions at once causes destructive interference between the channels. $\{\pi, \sigma^\pm\}$ and $\{\sigma^\pm, \pi\}$ are possible allowed transitions.

transition paths then reads

$$\Omega_{\text{eff}}(m_3, m_4) = \frac{1}{2\Delta} \sum_{F'=3}^4 \sum_{m'=-1}^1 \Omega_{3,m_3 \rightarrow F',m'} \cdot \Omega_{4,m_4 \rightarrow F',m'}^* \quad (3.7)$$

The sum over the possible excited states F' does not include $F' = 2$ and $F' = 5$, because due to the basic selection rules one of the matrix elements of the product is always zero. It should be emphasized that the matrix element for a single transition will always be a real number in this notation through a common phase convention [18]. Hence the coupling strength connecting m_3 to m_4 is the same as the one connecting m_4 to m_3 .

The selection rules for Raman transitions arising from interference effects can now be derived from the calculation of the matrix elements. The rules will depend on the chosen polarization of the light and the chosen quantization axis for the magnetic sub states. As already mentioned, due to the limited optical access it is not possible to shine in the Raman beams from all directions with desired polarizations. I will therefore restrict the discussion to the relevant cases.

In order to know which polarization of light will drive what kind of transition one has to decompose the electric field into the well known basic cases: Linear polarized light will drive π transitions if the quantization axis points in the direction of the electric field of the light. Right/left-circularly polarized light will drive σ^- and σ^+ transitions when the

3.1 Theory of Stimulated Raman Transitions

quantization axis points into the direction of the propagation of the light. In the experiment both Raman beams are right handed circularly polarized. The quantization axis is given by an external magnetic field and has the two configurations: along the propagation axis (II) and perpendicular (X) to it.

Parallel B-Field

For the II case the situation coincides with a basic case. B-field and propagation of light point in the same direction from now on called y . The light will drive $\{\sigma^-, \sigma^-\}$ transitions, where in this notation the first entry corresponds to the one-photon transition of the pump laser, and the second entry denotes the one photon transition of the stokes laser. The pathways over the possible excitation routes $F' = 3, 4$ will interfere constructively for this configuration.

Perpendicular B-Field

For the X-case one can split the electric field of the light into its contributions in the following manner:

$$\begin{aligned} \mathbf{E}(t, y) &= E_0 e^{-iky} e^{-i\omega t} \frac{1}{\sqrt{2}} (\mathbf{e}_z - i\mathbf{e}_x) \\ &= E_0 e^{-iky} e^{-i\omega t} \left(\underbrace{\frac{1}{\sqrt{2}} \mathbf{e}_z}_{\frac{1}{\sqrt{2}}\pi} - \underbrace{\frac{i}{2\sqrt{2}} ((\mathbf{e}_x + i\mathbf{e}_y) + (\mathbf{e}_x - i\mathbf{e}_y))}_{-\frac{i}{2}(\sigma^+ + \sigma^-)} \right) \end{aligned} \quad (3.8)$$

The right handed circular polarized wave can be seen as a superposition of two linear polarizations with a relative phase delay of $\pi/2$. The contribution pointing in the direction of the quantization axis will drive π -transitions. The perpendicular part however can be seen as a superposition of right and left circular polarized light in the x-y-plane. Effectively, of course, there is no contribution of the electric field in the direction of propagation (y). The linear perpendicular part will therefore drive σ^+ and σ^- transitions with equal strength. Half of the power of the light drives π transitions and a quarter of the power σ^+ transitions and σ^- transitions each. All combinations of σ^+ , σ^- and π transitions are then driven simultaneously, with the circular contributions having a phase delay of $\pi/2$ with respect to the linear part. By calculating the coupling strengths for all combinations of $\{\pi, \sigma^+, \sigma^-\}$, one can see the following selection rules emerging.

- For $m_4 - m_3 = \delta m = 0$ the following routes interfere: $\{\pi, \pi\}$, $\{\sigma^+, \sigma^+\}$ and $\{\sigma^-, \sigma^-\}$. The coupling of $\{\pi, \pi\}$ transitions itself is zero due to interference between the couplings to $F' = 3, 4$. $\{\sigma^+, \sigma^+\}$ and $\{\sigma^-, \sigma^-\}$ itself are non-zero but of equal magnitude and opposite sign, and therefore cancel each other. Hence all $\delta m = 0$ transition are suppressed.

3 Stimulated Raman Transitions of a Few Atoms

- For $\delta m = \pm 1$ the following transitions interfere: $\{\sigma^\pm, \pi\}$ and $\{\pi, \sigma^\pm\}$. Here both paths add up. The phase difference of $\frac{\pi}{2}$ between π and σ^\pm has no influence, since it is the same for both pairs.

3.2 Push-Out Technique

In order to detect the stimulated Raman transitions it is necessary to measure the hyperfine state of the atoms. In order to do so, the so called push-out technique is used and shall shortly be presented here. The dipole trap is far detuned from any atomic transition, and thus hyperfine state changing scattering of photons from the dipole trap can be neglected. When the atoms are loaded into the dipole trap they therefore stay in the ground state in which they are prepared during the loading process. By turning of the repumping laser of the MOT after the molasses beam, the atoms can be prepared in the $F = 4$ state. The Raman beams are then turned on for a fixed pulse length. After the pulse the atoms are in a superposition of the ground states and thus have a probability to be detected in either of them. It is now possible to destructively detect the internal state by the so called push-out technique [19]: A laser resonant with the $F = 4$ to $F' = 5$ transition is applied perpendicular to the DT. When the atom is in $F = 4$ state the atom is pushed out of the trap by the radiative pressure of the beam. An atom in the $F = 3$ state is unaffected by the laser and remains inside the trap. By loading the atoms back into the MOT and counting their number again the number of atoms in $F = 3$ can be deduced.

3.3 Spectra

3.3.1 Setup

As it turned out, the alignment of the Raman beams onto the the dipole trap seems to be crucial to get a good performance of the system. With the help of a beam-profile camera and by deflecting all beams before the vacuum cell onto the camera it is possible to align the beams onto the position of the MOT and the cavity inside the vacuum cell. The resulting geometry of the Raman beams is shown in figure 3.3. While the focus of the dipole trap is approximately one millimeter in front of the cavity the focus of the Raman beams is 14 mm behind the cavity. The beam waist ($1/e^2$) at the position of the MOT and at the waists at the position of the cavity are

	MOT	Cavity
Raman	102.5 μm	85.5 μm
DT	44.5 μm	36 μm

It can be seen from images taken of atoms with an imaging system [20], that the atoms are radially confined in the dipole trap within a radius of about 4 μm . It is crucial that different atoms inside the dipole trap see approximately the same intensity of the Raman

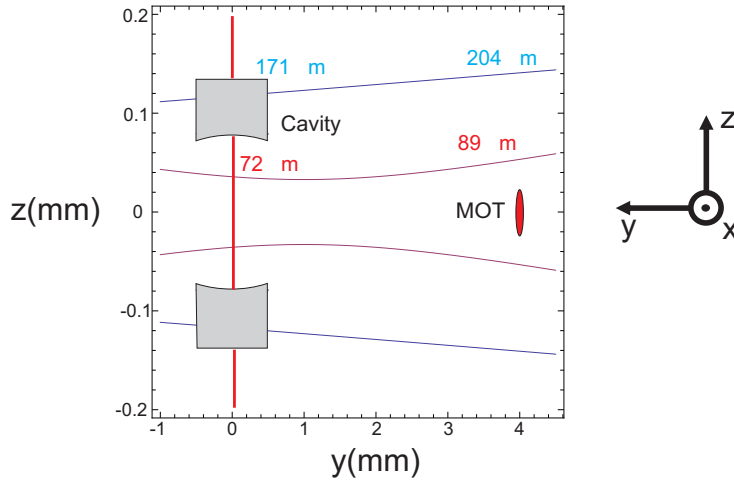


Figure 3.3: An up-to-scale drawing of Raman beams, dipole trap, MOT and cavity. The elongation of the MOT in the y direction is slightly enhanced in order to see it. The cavity mode inside the cavity has a waist of $40 \mu\text{m}$ and is also slightly enhanced. The cavity length in z direction is $158 \mu\text{m}$. The diameters of dipole trap and Raman beams are given in the drawing.

beams, in order to avoid inhomogeneous dephasing effects. The waist of the Raman beams is therefore chosen to be larger than the waist of the dipole trap in order to illuminate the atoms homogeneously. With the given waist of the Raman beams at the position of the MOT and assuming that the atoms are located at the center of the Gaussian beam, different atoms moving inside the trap would see a variation in intensity of around 0.3%. In addition to that, it might also be that back-reflections from the cavity holders generate inhomogeneities in the intensity profile of the Raman beams. The dipole trap was therefore operated at maximum power and with that maximal trap depth in order to localize the atoms strongly. With these settings it is possible to get the best results. The earth's magnetic field and residual magnetic fields from other parts of the laboratory are compensated with compensation coils.

3.3.2 Spectra of Zeeman-Sublevels

As the first experimental step, spectra of the magnetic substructure are taken. The degeneracy of the magnetic substates is lifted by the Zeeman effect induced by an externally applied magnetic field. Spectra were recorded for two possible quantization axes II and X. The B-field strength is chosen in a range, that the splitting of the outermost Zeeman-sublevels is on the order of 2 MHz. The pulse length is fixed to $20 \mu\text{s}$ and the power of both beams is $600 \mu\text{W}$, equally split between Stokes and pump beam. The one-photon detuning is $\Delta = 320 \text{ GHz} \cdot 2\pi$. For these parameters we can roughly expect to have a two-photon Rabi frequency in the range of kilohertz, comparable to microwave transitions. With the

3 Stimulated Raman Transitions of a Few Atoms

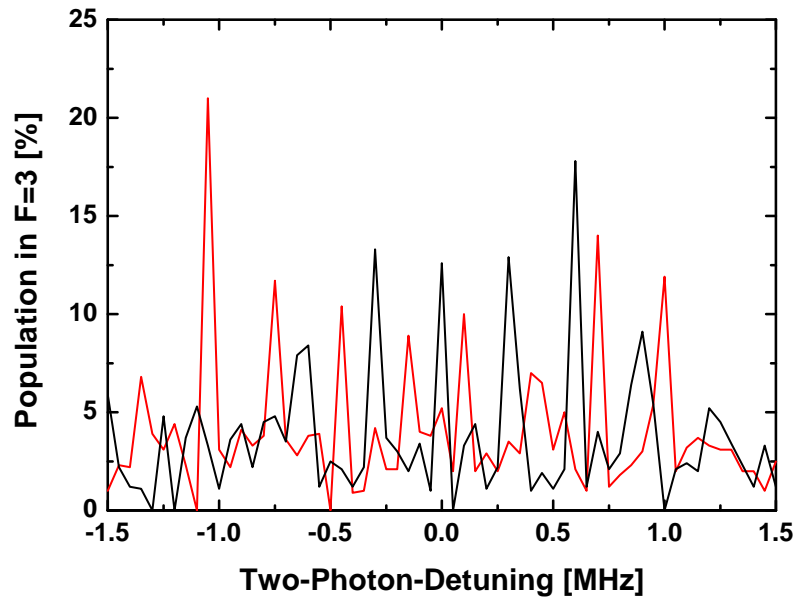
short pulse length of $20 \mu\text{s}$, we expect to be below the pulse duration for the π -pulse condition, corresponding to a full population transfer from $F = 4$ to $F = 3$. For each detuning 5 shots with around 15 atoms each are recorded. The spectra are shown in 3.4(a), given in population transfer to the $F = 3$ state in percentage. The height of the peaks depends not only on the coupling strength but also on the numbers of atoms prepared in each magnetic sub level. Since the m_4 distribution in the $F = 4$ level after the preparation process is not well known, the amplitude of the peaks is hard to interpret and will not be investigated. For the II distribution 7 peaks are expected corresponding to the $\{\sigma^-, \sigma^-\}$ transitions of the seven ground m_3 states. Clearly visible are only 6. A reason for the missing $m_4 = -3$ to $m_3 = -3$ transition that is expected to be in the range of $\delta = -1.2.. - 0.8$ MHz might be attributed to optical pumping into other m_4 states during the preparation process. The outermost $m_4 = \pm 4$ states are dark for the light.

For the magnetic field perpendicular(X) to the dipole trap axis however $\delta m = \pm 1$ transitions are now allowed. The $m_4 = x$ to $m_3 = x + 1$ transition has the same detuning as the $m_4 = x + 1$ to $m_3 = x$ transition for $x = -3, \dots, 2$. Hence of the 14 possible transitions 12 detunings occur pairwise degenerated resulting in $6+2=8$ peaks. The 8 peaks can clearly be identified symmetrically spread around $\delta = 0$. The linewidth of the peaks is on the order of 60 kHz as is expected from the Fourier limit arising from the finite pulse length given by

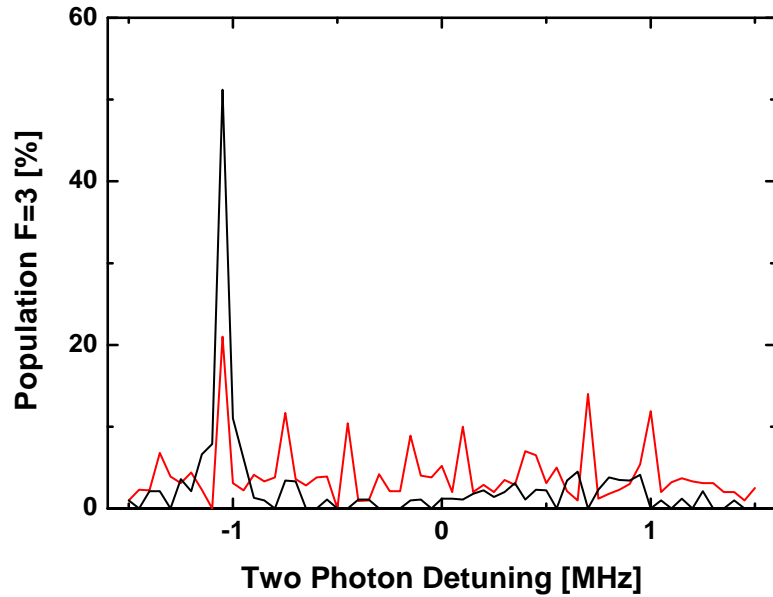
$$\delta\nu = \frac{1}{20\mu\text{s}} = 50 \text{ kHz.} \quad (3.9)$$

3.3.3 Optical Pumping

In order to prepare the atoms in a single magnetic substate the atoms are optically pumped. In this situation the system is a real two-level system since all atoms have the same effective coupling strength corresponding to that transition. In this situation one is not sensitive to the m_4 distribution after the loading into the dipole trap anymore. The optical pumping is done by applying a B-field in y-direction (II) after the atoms are loaded into the dipole trap. A right handed circular polarized optical pumping beam resonant with the $F = 4$ to $F' = 4$ transition is applied. During this process a repumping laser resonant with the $F = 3$ to $F' = 4$ is as well applied to keep the atoms in the $F = 4$ manifold. The atoms are then pumped into the $m_4 = -4$ state, which is a dark state for the pumping laser. Now the B-field is rotated in the z direction, in order to apply the Raman pulse. If the rotation is done slowly compared to the lamor frequency the atoms will stay in their m_4 sub state. The quantization axis is now perpendicular (X) to the propagation axis and the outermost state is not a dark state for the Raman pulse anymore. The spectrum is shown in figure 3.4 (b). The black curve with optical pumping and the red one without. By comparing the pumped and the unpumped spectrum it is now also possible to clearly identify the outermost peak in the unpumped spectrum. An estimation for the B-field that is lifting the degeneracy of the magnetic substates can be made via the formula for the



(a)



(b)

Figure 3.4: (a) Spectrum for X (red) and II (black) configuration given in population transfer into F=3. (b) Spectrum for X configuration with optical pumping (black) and without (red) given in population transfer into F=3.

3 Stimulated Raman Transitions of a Few Atoms

Zeeman splitting by

$$B = \frac{\Delta E}{\mu_B(m_3g_3 - m_4g_4)} = \frac{h \cdot 1 \text{ MHz}}{(7/4)\mu_B} = 0.41 \text{ G} \quad (3.10)$$

for $m_3 = 3$, $m_4 = 4$, $g_3 = -1/4$ and $g_4 = 1/4$.

This preparation of a pure two-level system now allows us to induced Rabi oscillations between these states.

3.4 Raman-Rabi Oscillations

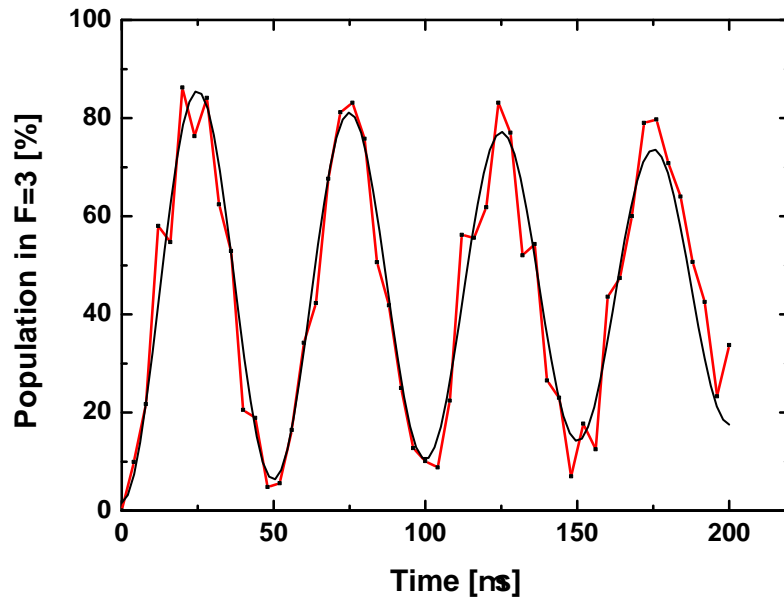
Rabi oscillations in a two level system are a standard problem [21]. The probability of finding an atom in $m_3 = -3$, when it was prepared in $m_4 = -4$, will oscillate with the effective coupling strength $\Omega_{\text{eff}} = \sqrt{\Omega_0^2 + \delta^2}$. Assuming no damping the probability then reads

$$p_{m_3=-3}(t) = \frac{\Omega_0^2}{\Omega_{\text{eff}}^2} \left| \sin \left(\frac{\Omega_{\text{eff}}}{2} \cdot t \right) \right|^2 \quad (3.11)$$

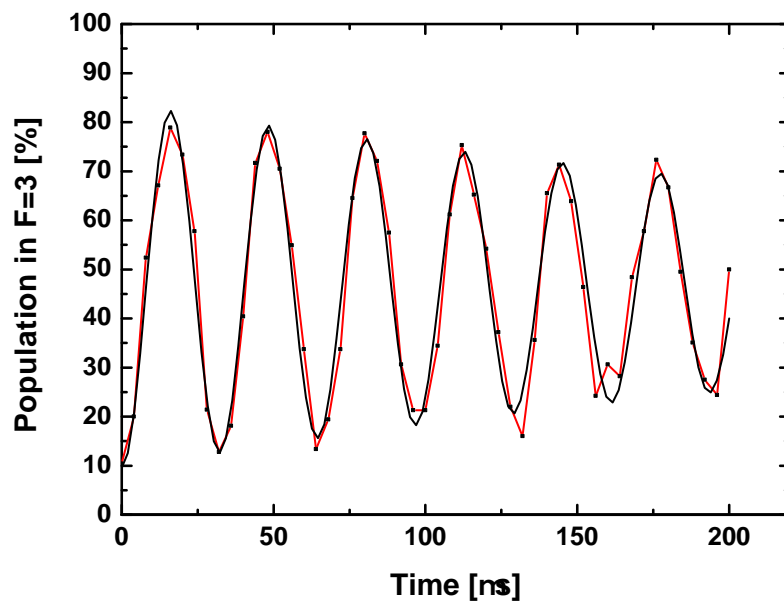
After taking a spectrum first, we know exactly the resonance frequency of the transition, which primarily is determined by the Zeeman effect. However also differential light shifts of the hyperfine levels arising from different coupling strengths of the laser could move the resonance frequency. By driving the Rabi oscillations on resonance of the with the peak we compensate all these effects and the effective two-photon detuning is zero $\delta = 0$. The power in both laser beams is 1000 μW , again equally split between the lasers. The one photon detuning is $\Delta = 169 \text{ GHz} \cdot 2\pi$. The population measured to be in $F = 3$ for different pulse lengths up to 200 μs is shown in 3.5(a). In order to extract the frequency the following function with a exponential damping term modeling the damping of the oscillations is fitted to the data:

$$P_3(t) = A(1 + e^{-t/\tau} \sin(\Omega_{\text{eff}} \cdot t)), \quad (3.12)$$

resulting in ($A = 43 \pm 3\%$), ($\Omega_{\text{eff}} = 19.89 \pm 0.06$) $\text{kHz} \cdot 2\pi$ and $\tau = (435 \pm 130) \mu\text{s}$. The expected flopping frequency was also calculated by the method explained in the theoretical section in the following way: The transition is driven by $\{\pi, \sigma^-\}$ and $\{\sigma^+, \pi\}$ transitions at the same time, since each laser drives $\{\pi, \sigma^+, \sigma^-\}$ transitions simultaneously. The electric field for the π transition is reduced by $1/\sqrt{2}$ and the σ^\pm contribution is reduced by $1/2$. The result for the geometrical contribution is $C = (\sqrt{7}/12 + \sqrt{7}/12)$. I assume that both lasers have the same power, but only 76% of the power actually drive the transition. This results from the way the lasers are locked and will be explained in chapter 4. The calculated Rabi frequency then reads



(a)



(b)

Figure 3.5: (a) Rabi oscillations induced via stimulated Raman-transitions up to a pulse length of 200 μs . (b) Rabi oscillation induced by microwave transitions up to 200 μs .

3 Stimulated Raman Transitions of a Few Atoms

$$\begin{aligned}\Omega_{\text{eff}} = \Omega_0 &= 0.76 \cdot \frac{1}{2\sqrt{2}} \frac{E^2 \cdot \frac{\sqrt{7}}{6} \langle J = 3/2 || er || J = 1/2 \rangle^2}{\hbar^2 \cdot 2 \cdot 169 \text{ GHz} \cdot 2\pi} \\ &= 0.76 \cdot 36 \text{ kHz} \cdot 2\pi = 27 \text{ kHz} \cdot 2\pi \\ E = \sqrt{\frac{2I}{c\epsilon_0}} \quad I(r=0) &= \frac{2P}{\pi\omega^2(z)} = \frac{2 \cdot 500 \mu\text{W}}{\pi \cdot (102 \mu\text{m})^2}.\end{aligned}\tag{3.13}$$

This difference from the calculated frequency and the observed one would lead to the assumption that only 72% of the measured light actually reach the atoms. The power is measured at some point before the vacuum cell, and there might be some small losses on mirrors and on the surface of the glass cell itself. These losses are however assumed to be small. Another reason could be a not perfect alignment. The atoms actually would not see the maximum intensity of the Gaussian beam profile of the Raman beam. Also inhomogeneities due to reflections could be the reason for a smaller intensity seen by the atoms. The contrast of the oscillation $2A$ is due to the back and forth loading efficiencies between the MOT and dipole trap. The efficiency of the push-out technique, i. e. the atoms in $F = 3$ who survive the pushout, was measured to $(91 \pm 2.5)\%$ and is in good agreement with contrast of the oscillation.

The damping of the oscillations however is a complicated mixture of many contributions and cannot be evaluated in detail with the present data. In order to get a rough estimation for the damping of the oscillations the simple form of an exponential damping was assumed in the model of the fit. Since the fit is only done for a few oscillations the error is rather large, and the estimated value is rather uninformative. For longer pulses than the one shown in 3.5(a) the envelope of the oscillations is not an exponentially damped curve anymore. In order to extract more information about the damping of the curve one would have to rely on more elaborate measurement concepts like Ramsey spectroscopy or the spin echo technique. There, inhomogeneous effects and homogeneous dephasing effects could be distinguished. Rabi oscillations induced by microwave radiation have proven to be a reliable tool in our experiment and their dephasing and decoherence processes were extensively studied in the thesis of Stefan Kuhr and published in [19]. It seems therefore reasonable to compare the Raman-Rabi oscillations with the microwave oscillations, in order to get a rough idea about the performance of the damping. A microwave oscillation with roughly the same frequency as the Raman-Rabi frequency was recorded, the measurement is shown in 3.5(b). Here the fit resulted in a damping of $\tau = (365 \pm 77)\mu\text{s}$. The finite population transfer for zero pulse length is due to an imperfection of the push-out technique for that recorded data set. It can be concluded that for the first few oscillations the damping is of the same order. With this result the performance of the Raman-setup was declared to be sufficient enough to proceed with the main experiment.

It however can be noticed that many of the dephasing and decoherence effects the damping of the microwave oscillations will be the same source as for the damping of the

Raman-Rabi oscillations. The main source for inhomogeneous dephasing is: The thermal distribution of the atoms in the dipole trap. The atoms see a different differential light shift induced by the dipole trap, which results in different Rabi frequencies for the atoms, which shows up as damping in the averaged measured Rabi oscillation. This is an inhomogeneous dephasing effect. Other homogeneous sources for the dephasing are: Instabilities in power and alignment of the dipole trap, which again would show up as fluctuations in the differential light shift. Fluctuations in the magnetic field. Decoherence by scattering of photons from the dipole trap can as well damp the oscillations. This effect however can be neglected.

For the Raman-setup additional an additional source of dephasing might be: Incoherent scattering of photons from the Raman-beams. With the fitted coupling strength for the Raman-Rabi oscillation and assuming the same coupling strength for pump and Stokes beam, one can get an estimation for the single coupling strength for the one-photon transition by

$$19 \text{ kHz} \cdot 2\pi = \frac{\Omega^2}{2\Delta} \quad (3.14)$$

\Rightarrow

$$\Omega = \sqrt{2 \cdot 2\pi \cdot 19 \text{ kHz} \cdot 2\pi \cdot 169 \text{ GHz}} \approx 80.1 \text{ MHz} \cdot 2\pi.$$

With this coupling strength the scattering rate for a large detuning from the atomic resonance frequency detuning can be calculated by

$$\Gamma_{\text{Scat}} = \frac{\Gamma \Omega^2}{4 \Delta^2} = \frac{2\pi \cdot 5.2 \text{ MHz} (2\pi \cdot 80.1 \text{ MHz})^2}{4 (2\pi \cdot 169 \text{ GHz})^2} = 18.3 \frac{1}{s} \quad (3.15)$$

and thus the influence is very small for our pulse lengths in the μs range. Possible further sources of noise might be power and pointing instabilities and in the Raman beams. Also the influence of the phase lock is not understood.

It also has to be mentioned that it is possible to move the atoms inside the cavity and drive the Raman transitions there and then move the atoms back, and do the push out measurement. This worked, and thus the Raman setup can as well be used to manipulate the internal states of the atom inside the cavity. This was not possible with the microwave transitions, because so far they disturb the locking mechanism of the cavity.

3.5 Conclusion

To sum up, it was possible to integrate the Raman-setup into the main experiment and by aligning it carefully with the axis of the dipole trap it was possible to drive stimulated Raman-transitions in atoms caught in the dipole trap. The damping of Rabi oscillations

3 Stimulated Raman Transitions of a Few Atoms

could be minimized to a degree that it seems reasonable to proceed and use the setup in combination with the cavity. In foresight to do this the beams are already aligned to the cavity. However, it has to be said that in order to investigate the performance of the Raman setup more closely, much more systematic measurements have to be done. The behavior of the oscillations for higher Rabi frequencies, which would be needed to drive cavity-Raman-transitions, was not been yet investigated,

4 Performance of the Optical Phase Lock Loop

The strong damping of the first recorded Raman-Oscillations raised the question, if the performance of the OPLL itself is a limiting factor to the quality of the oscillations. I therefore spend a considerable amount of time on characterizing the performance of the lock. By observing the so called quadrature signal I implemented a new additional analysis tool to the setup. This will provide more reliable information about the performance of the lock. This tool can as well be used to investigate possible arising problems with the lock in the future. As a consequent step I also looked for possibilities to further increase the quality of the lock. This task was rather unsuccessful but motivated a more detailed analysis of the single lock constituents. By observing the frequency modulation response of the lock constituents separately it was possible to identify the limiting factors of the current system, mainly the lasers themselves.

4.1 Characterization of the Phase Noise

The declared goal of an OPLL is to stabilize the optical phase emitted by the slave laser ϕ_S with respect to the optical phase of the light emitted by the master laser ϕ_M . In the experiment however, the lock is used to stabilize two lasers to a desired frequency difference. The stability of the frequency difference is the crucial parameter of the system, not the absolute frequencies of the lasers. As described in chapter 2, the frequency offset is adjusted by the sum of two local oscillators (LO1+LO2) that demodulate the frequency offset from the beat signal. A phase detector (PFD) then provides an error signal related to the phase difference between the master and the slave laser. For a perfect lock the phase difference would be zero and the laser would run with with a perfectly fixed frequency difference. In reality the phase difference fluctuates around a mean value. This leads to their frequency components in the beat signal. Understanding the structure and strength of this broadening is therefore crucial in order to describe the performance of the lock.

4.1.1 Beat Signal

First of all, it has to be said that the feedback signal changes the current of the laser and thus the frequency of the laser. The feedback signal generated by the PFD however is proportional to the phase difference between the two lasers and can then be seen as a sinusoidal modulation of the laser frequency with different frequencies. Since phase and frequency are related by $\phi = \int \omega dt$ a sinusoidal modulation of the laser frequency translates

4 Performance of the Optical Phase Lock Loop

in a modulation of the phase

$$\phi_S(t) - \phi_0 = \int_0^{t'} \omega_S \cos(\omega_{\text{mod}} t) dt = \omega_S \left[\frac{1}{\omega_{\text{mod}}} \sin(\omega_{\text{mod}} t) \right]_0^{t'} = \frac{\omega_S}{\omega_{\text{mod}}} \cos(\omega_{\text{mod}} t - \pi/2) \quad (4.1)$$

but with a phase delay of $\pi/2$. When both lasers are *phase* locked the *frequency* difference will be exactly fixed. The modulation of the phase difference, however, will create sidebands to this carrier frequency. After all, phase and frequency are just two sides of the same medal, and one can always switch between the two. I will now stay in the phase picture.

The beat signal that is amplified after the fast photodiode was given in 2.1 by

$$\text{Beat}(t) = A \cos((\omega_M - \omega_S)t + \phi_M(t) - \phi_S(t)) \quad (4.2)$$

Since the current is modulated in order to change the frequency and thus the phase of the slave laser also the amplitude of the beat signal will be modulated. Both phase modulation and amplitude modulation will create sidebands to the carrier frequency.

A spectrum of the beat signal is recorded with a spectrum analyzer. In figure 4.1 a typical spectrum of the beat signal is shown. The linewidth of the center carrier peak is only limited by the resolution bandwidth of the spectrum analyzer and expected to be a delta peak. Noise infinitesimal close to the carrier peak would correspond to infinite slow modulations of the phase difference between the local oscillator sources and the phase of the beat signal. It is not expected that these very slow modulations should show an increase in amplitude for very slow oscillation, since the lasers are phase locked. Hence there will be no increase in the noise for frequencies arbitrarily close to the carrier frequency. The characteristic bumps, that are around 2 MHz away from the carrier, are called servo bumps and are caused by the finite bandwidth of the feedback loop. Higher frequencies of modulations on the phase difference induced by noise cannot be compensated by the feedback loop. Here the feedback becomes positive and causes swinging. The slaver laser will be modulated with this swinging frequency and the sidebands become visible in the spectrum. The bumps around 1.1 MHz away from the carrier are attributed to noise picked up by the lock from the laboratory. The source of this noise could not be located by the end of the thesis. The spectrum however does not provide any information on the time evolution of the phase difference or the type of the sidebands, amplitude or phase modulation.

4.1.2 Quadrature

In order to investigate the time evolution of the beat signal, the so called quadrature signal of the beat signal was recorded. The simple setup for this measurement is shown in figure 4.2. The down converted beat signal is split and mixed again with the local oscillator (LO 2) source that is providing the reference for the PFD. The sum frequency contribution is suppressed by a low-pass. When the lasers are locked, the frequency difference between the down converted beat signal and the LO 2 signal will be zero, and the output will be proportional to $A \cos(\phi_S(t) - \phi_M(t))$. Here the phase of the local oscillator is set to $\phi_{LO} = 0$.

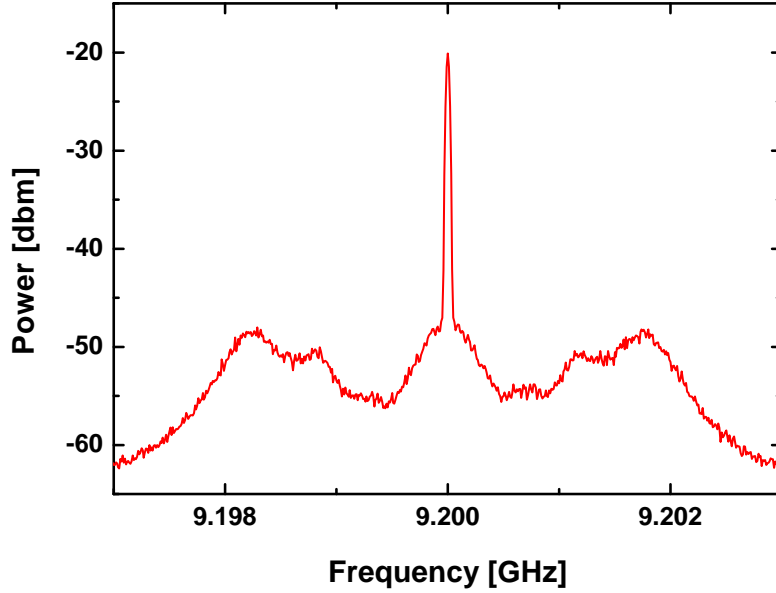


Figure 4.1: Spectrum of beat signal between a free running master laser and phase locked slave laser recorded with a spectrum analyzer (RBW=30kHz). The frequency offset of the slave laser is fixed to 9.2 GHz, determined by the frequency of the sum of the local oscillators (LO1+LO2). Characteristic servo bumps, originating from the finite bandwidth of the lock, can be seen close to 2 MHz away from the carrier. The smaller bumps around 1.1 MHz are attributed to noise.

This will provide an in-phase channel with the local oscillator signal named I. Adding a phase shift of π to the LO signal, yields a signal proportional to $A \sin(\phi_S(t) - \phi_M(t))$, this channel is out of phase by $\pi/2$ with the local oscillator signal and is named quadrature Q. The phase delay was created by choosing different BNC cable lengths between LO 2 and the two mixers.

From these two channels the time evolution of the phase difference can be extracted in the following way: Plotting Q vs. I in figure 4.5(b)(a) and (b) shows two typical signals. In principle this should be the circle and amplitude and argument of the two channels are given by

$$A^2 = Q^2 + I^2 \quad (4.3)$$

$$(4.4)$$

$$\text{and} \quad (4.5)$$

$$(4.6)$$

$$\arctan\left(\frac{Q}{I}\right) = \arctan\left(\frac{\sin(\phi_S(t) - \phi_M(t))}{\cos(\phi_S(t) - \phi_M(t))}\right) = \phi_S(t) - \phi_M(t) \quad (4.7)$$

4 Performance of the Optical Phase Lock Loop

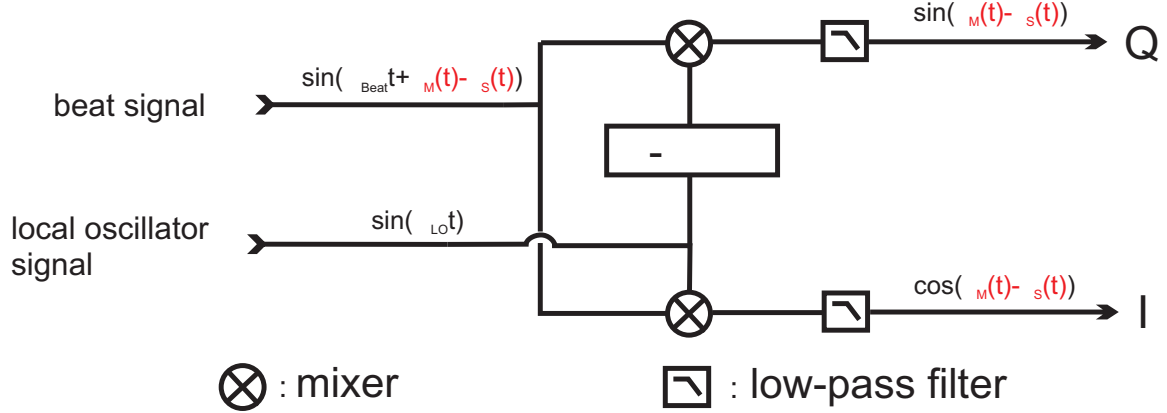


Figure 4.2: Beat signal and local oscillator frequency are mixed. In case of locked lasers the frequencies of beat signal and LO 2 source are equal the mixing gives an in-phase signal proportional to $A \cdot \cos(\phi_S(t) - \phi_M(t))$ named I. Adding a phase delay of $\pi/2$ to the local oscillator source and mixing it with the beat signal will give an $\pi/2$ out phase signal proportional $A \cdot \sin(\phi_S(t) - \phi_M(t))$ named quadrature Q.

The not perfect circular shape in the data originates from the phase delay that is not exactly $-\pi/2$. The phase and amplitude can now be extracted from these signal by fitting an ellipsis to the data and using an algorithm to detect phase deviations larger than $\pm\pi$ from the mean value of the phase. In 4.5(b)(c) the extracted phase for a perfectly adjusted lock is shown and in (b) where the lock is forced to swing due to a too large current feedback. For the perfect adjusted lock no phase deviations occur that would force the PFD to switch into frequency detection operation. If such a larger phase deviation would appear a so called cycle slip could occur. The swinging case provides a test for the the algorithm to detect these possible slips in phase. The too strong current feedback will create a forced phase deviation larger than π . The PFD will switch into frequency detection operation mode and the phase deviation can not be corrected. The reference phase by the master laser however is still given and the slave laser will fall back into lock, but now with a phase deviation of 2π , the cycle slip occurred. The jumps in phase by multiplies of 2π can be seen in (d). This information could not be deduced from the spectrum, and can now be ruled out as a possible source for disturbances when the Raman setup is used.

Furthermore, it is now possible to directly determine the broadening of the phase deviation described by the RMS value of the phase deviations. For our setup the broadening also depends on the laser chosen to be the master laser. For the free running master laser that was used to drive the Rabi oscillations the RMS value for the phase deviation is calculated from 200 shots to $(0.52 \pm 0.0025)rad \equiv 29^\circ \pm 0.1^\circ$. In contrast for the the EIT measurement the probe laser of the main experiment serves as the master laser. This laser does not pick up the noise that can be seen as a peak 300 kHz away from the carrier

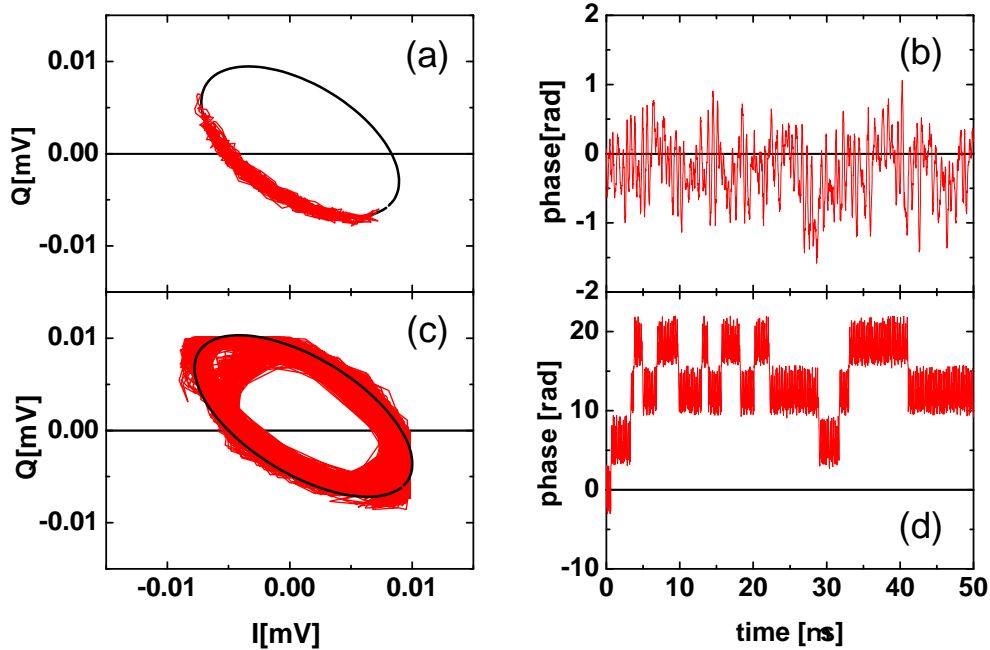


Figure 4.3: (a): QI-signal for optimal lock settings, with fitted ellipsis (b) Extracted phase from QI-signal in figure (a). (c): QI-signal for a swinging lock (d): Exctrated phase from QI-signal in (c).

in 4.4 (a), which shows a recorded beat signal corresponding to the laser that was used for the stimulated Raman transition measurements. Hence its performance is better. In addition to this probe laser is locked to a polarization spectroscopy. For the case of locked probe laser the phase deviation becomes larger due to a disturbance acting on the OPLL induced by the spectroscopy lock. The spectroscopy lock will amplify noise in the relevant frequencies regions of the phase lock, that are irrelevant for the spectroscopy lock. The resulting phase deviations are for the unlocked case $(0.42 \pm 0.002)rad \equiv 24^\circ \pm 0.1^\circ$ and $(0.44 \pm 0.002)rad \equiv 25^\circ \pm 0.1^\circ$ for the locked case. With the knowledge of the phase deviation it is now also possible to determine the fraction of power in the carrier of the beat signal. The fraction is related to the phase deviation by [22]:

$$\frac{P_{\text{carrier}}}{P_{\text{total}}} = e^{-\phi_{\text{RMS}}^2} \quad (4.8)$$

This results in a fraction of 76% of power in the carrier for the free running master laser and 82% and 83% for the locked and free running probe laser of the main experiment. In principle one could also integrate the area under the beat signal and compare it to the power in the peak, but this method is not as trustworthy since the area under the spectrum strongly depends on the resolution bandwidth of the spectrum analyzer, while the power in the carrier is quite insensitive to the resolution.

It is also possible to determine what the source of the spectral broadening is. One can

4 Performance of the Optical Phase Lock Loop

now distinguish if the sidebands occur dominantly from amplitude or phase noise. To show the relation between the spectrum recorded with the spectrum analyzer and the quadrature measurement, the autocorrelation function of the phase of the beat signal averaged over 200 shots of sample length $50\mu s$ is calculated. The autocorrelation function I used for the discrete samples is

$$R(l_\tau) = \frac{1}{SL_{\tau_{max}} - l_\tau + 1} \sum_{i_t=1}^{SL_{\tau_{max}} - l_\tau + 1} \phi_{i_t} \phi_{l_\tau + i_t - 1} \quad (4.9)$$

where $SL_{\tau_{max}}$ is the sample length corresponding to the maximal τ that can be calculated. The values for the largest τ are neglected since their sum is just taken over a few sample points resulting in a bad signal-to-noise ratio. According to the Whiner-Khintichine-Theorem [23] the Fourier transform of the autocorrelation function of the noise is the spectral density of the noise. The power density of the Fourier transform was calculated with the help of Origin.

The spectrum recorded with the spectrum analyzer, the autocorrelation function and the calculated spectral density are shown in figure 4.4. The DC-term of the Fourier transform has no meaning since it corresponds to the the offset of the auto correlation function. Since the zero point of the phase can be chosen arbitrarily, the offset of the autocorrelation carries no physical information. The power density of the Fourier transform however was normalized to the DC-term. In the plot the dbc scale therefore only serves as logarithmic scale. The calculated spectral density of the phase noise can now be compared to the spectrum of the beat signal recorded with the spectrum analyzer, where the noise appears as sidebands to the carrier frequency. The shape of the noise is clearly reproduced and one can therefore conclude that the main source for broadening is the phase noise and not possible amplitude fluctuations. The resolution of the calculated spectrum is limited by the length of the recorded traces of the phase and as well the time resolution of the traces of the phase. The spectral density of the amplitude noise was as well calculated but is not presented here, since it only picks up the noise that appears as the small peak at around 1.1 MHz. It is also not unexpected that the phase noise is the main broadening mechanism, since current changes that change laser frequency by a few megahertz are in the range of μA and thus very small compared to the operating current of the diode around 40 mA.

4.2 Theoretical Analysis of the Lock

In order to improve the lock performance I tried to implement a three-path feedback system, with one path acting on the grating, then the PFD acting as source for a current modulation input of the current controller of the slave laser, in order to maintain the high capture range of the digital element. For the third path the output of one of the mixers from the QI-setup was used as an error signal that directly modulates the laser current via the modulation input of the laser. I assumed that the mixer had less electronic noise than the PFD [24], which has to transform the analog signal into a digital one. This could

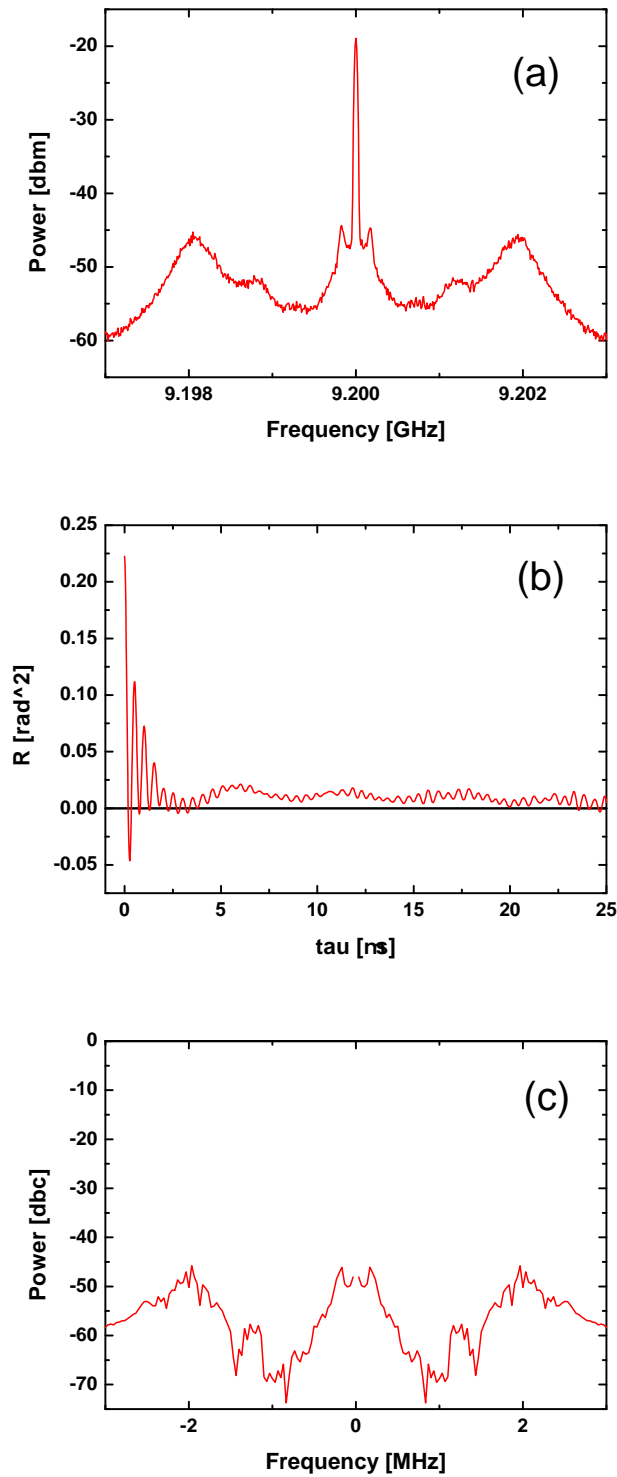


Figure 4.4: (a) Spectrum recorded with spectrum analyzer (RBW = 30 kHz). (b) Autocorrelation function of the phase difference, averaged over 200 shots with sample length $50\mu s$. (c) Calculated spectral noise density according to the Whiner-Khintichine-Theorem

4 Performance of the Optical Phase Lock Loop

be a possible noise source. It turned out that it is possible to lock the laser, but with no improvement to the existing setup. This might be due to the difficulty to adjust the three path feedback system to harmonize nicely, but also gave rise to the question, what the limitation of the system are. In order to do so the lock is first described in the theoretical context of control loop theory.

4.2.1 Control Theory

To describe the stability of closed feedback loop the concept of so called transfer functions is a useful tool. A transfer function is defined as [25]:

$$T(s) = \frac{X(s)}{Y(s)} = \frac{\mathcal{L}\{x(t)\}}{\mathcal{L}\{y(t)\}} \quad \text{with} \quad \mathcal{L}\{f(t)\} = \int_0^{\infty} e^{-st} f(t) dt \quad \text{and} \quad s \in \mathbb{C} \quad (4.10)$$

where \mathcal{L} is the Laplace transform of a signal, $x(t)$ before and $y(t)$ after a signal processing element. The advantage of transforming into Laplace space is that the transfer function of consecutive time invariant linear signal processing elements is the product of the transfer functions of the individual elements, and with this provides the possibility to analyze the lock by analyzing its constituents separately. The elements of a control loop can be summarized in the following categories: First the reference, that defines the desired output of the system, then a detector that measures the difference between the actual state of the system and the reference, than a controller (C), that has to process the error, and finally the dynamics of the system (S) that has to be controlled. A schematic sketch is shown in figure 4.5(a). In order to analyze the stability of the feedback loop one can use the relation between the open loop transfer function, i.e. the signal going one time through controller and system, and the closed loop transfer function, i.e. the complete system with feedback path closed given by this relation

$$G_{\text{open}}(s) = C(s)S(s) \quad G_{\text{closed}}(s) = \frac{C(s)S(s)}{1 + C(s)S(s)}. \quad (4.11)$$

The imaginary axis $s = i\omega$ of the transfer function corresponds to an experiment accessible quantity: The frequency modulation response of the element. The modulus of $|T(i\omega)|$ is the gain of a sinusoidal modulation ω modulating the system. The argument $\text{Arg}(\text{Tr}(i\omega))$ the phase shift of the modulation response of the system. In order to relate the frequency modulation response to the stability of the closed feedback loop the so called Nyquist stability criterion can be applied. The criterion exploits the relation between open and closed loop transfer function and identifies the modulation frequency where the phase shift of the open loop crosses $\text{Arg}(G_{\text{Open}}(i\omega)) = -180^\circ$, or the gain $|T(i\omega)|$ becomes smaller than one, as the largest noise frequency that can be compensated by the closed feedback loop. It is therefore possible to investigate the bandwidth of the lock without having the feedback loop closed and just measuring the frequency modulation transfer functions of the single elements

4.3 Measurement of the Frequency Modulation Response of the System

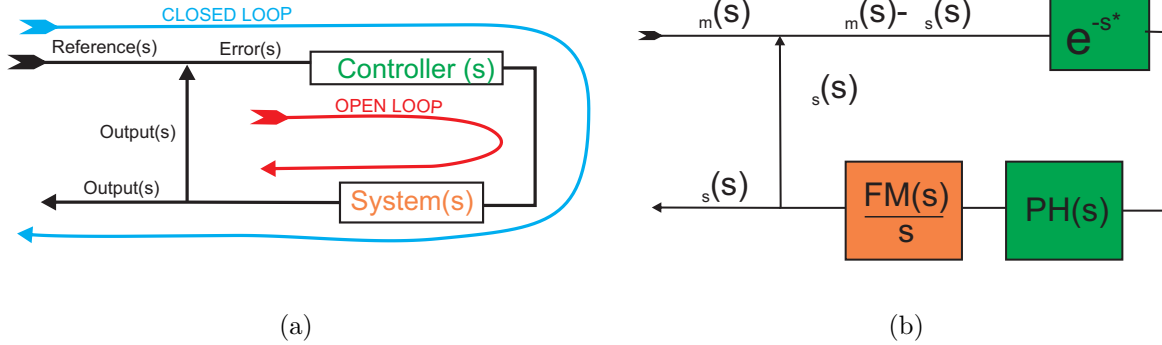


Figure 4.5: (a) Open and closed feedback loop, consisting of reference, error signal, controller, and system. (b) corresponding loop for the OpLL consisting of lead-lag filter and laser

4.2.2 Elements of the Optical Phase Lock Loop

In order to describe the OPLL via transfer functions, only the fast feedback loop modulating the laser current is considered, since this is the feedback determining the performance once the laser are locked. The controller and the system for the OPLL can be split in the following way,

$$C(s) = e^{-s\tau}PH(s) \quad S(s) = L(s) = \frac{FM_{Laser}(s)}{s} \quad (4.12)$$

where $e^{-s\tau}$ describes the finite time an error signal needs to propagate through the system, $PH(s)$ describes the system after the phase detector: The lowpass that averages the output of the PFD and the lead-lag filter. The system that needs to be controlled is the slave laser itself given by $L(s)$. The laser will be described by its frequency modulation response $FM_{Laser}(s)$ and an $1/s$ fraction term arising from the already mentioned fact, that a modulating of the laser current will change the laser frequency, the quantity that has to be controlled however is the optical phase. The additional added phase delay of 90° is reflected by the division by s . In the context of the transfer function the relation between $\phi = \int \omega dt$ in time space translates into a division by s for a Laplace transform.

4.3 Measurement of the Frequency Modulation Response of the System

In order to measure the frequency modulation response of the elements that make up the lock a so called network analyzer and a low finesse cavity as a frequency-amplitude discriminator are used. The cavity is built with simple planar dielectric mirrors in a triangle configuration. Its free spectral range and the FWHM value for the resonance line are

4 Performance of the Optical Phase Lock Loop

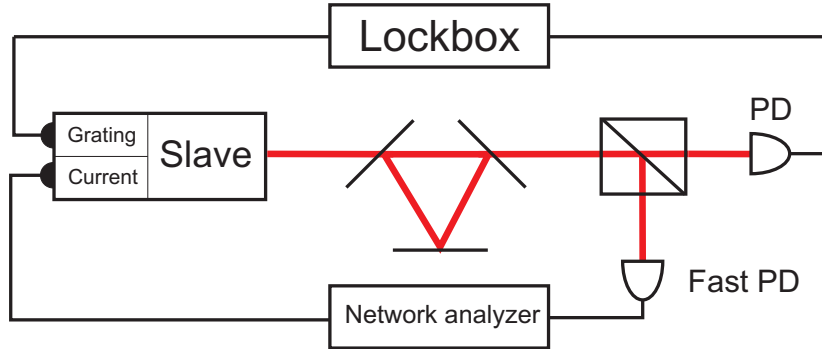


Figure 4.6: The cavity serves as a phase-frequency discriminator. The slave laser is locked onto the slope of the cavity transmission in order to give an stable reference transmission. The laser current is modulated by the network analyzer and the gain and phase delay of the modulation response is measured.

measured to ($\Delta_{\text{FSR}} = 234\text{MHz}$ and $\Delta_{1/2} = 25\text{MHz}$). The experimental setup is illustrated in figure 4.6. The slave laser current is modulated with a given frequency by the network analyzer. When the laser is tuned to the slope of the cavity transmission peak the cavity frequency modulation of the laser output translates into an intensity modulation output of the cavity. The intensity modulation is detected by a photodiode and the signal is fed back to the network analyzer, which measures phase shift and gain of the signal. Since the gain is given here by the photodiode, and that has nothing to do with the actual lock, the discussion will be restricted to the phase shift of the frequency response of the laser. In order to keep the laser on the slope of the cavity transmission, the laser is locked via the grating feedback onto the slope of the cavity transmission. The slow lock only compensates modulation frequencies below 10 kHz and thus is too slow to disturb frequency modulations in the interesting range from around 2 MHz. It however keeps the cavity transmission at a stable reference level. The cavity parameters are chosen in a way to give a feasible signal to lock the cavity, but also to be fast enough to neglect its influence on the phase of the modulation signal. One can think of the cavity as a low-pass with a cutoff frequency of 25 MHz. The phase lowering behavior of the low pass can be modeled and later numerically included in the measured data by

$$\phi_{\text{cavity}} = \arctan\left(\frac{\nu}{25 \text{ MHz}}\right) \quad (4.13)$$

The cavity transmission that is fed back to the network analyzer is recorded by fast a photodiode (Newport) that is able to detect intensity modulations up to 100 MHz. In order to check that the photodiodes' influence on the phase can be neglected I crossed checked the measurements by taking different types of photodiode. In order to calibrate the network analyzer carefully I replaced the optical path length by a BNC cable with

4.3 Measurement of the Frequency Modulation Response of the System

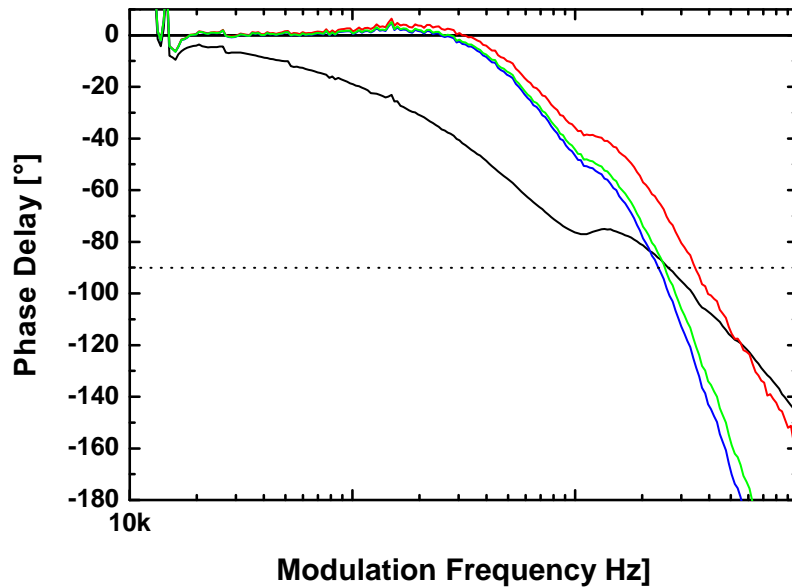


Figure 4.7: Phase of the frequency modulation response. The modulation frequency where the phase delay is -90° corresponds to the bandwidth of the lock. The black curve shows the bare response of the Laser. The red curve is with the added Lead-Lag filter. The lifting of the phase is increasing the bandwidth of the OPLL. The blue curve includes the phase delay by the finite loop time, decreasing the bandwidth. The green curve on top of all the before mentioned curves includes a model for the phase lowering effect arising from the frequency to intensity conversion in the cavity. The bandwidth can then be estimated to ≈ 2.5 MHz.

length $2/3$ of the optical path length, since it can be assumed that the speed of signal inside the BNC cable is $2/3$ of the speed of light. It is now possible to directly measure the frequency modulation response of the laser. The measured phase delay is shown in 4.7 and is the black curve. The interesting point in this plot is the frequency where the phase crosses -90° , since the -90° from the frequency modulation to phase modulation conversion still have to be added. The crossing of the -90° will thus determine the bandwidth of the complete optical phase lock loop.

4.3.1 Influence of the Thermal Response of the Laser Diode to Frequency Modulation

The complete current FM-response of the laser diode can be split into two contributions. The so called thermal contribution will dominate at low modulation frequencies. An increase in electrons in the diode will lead to a higher temperature, which then leads to a redshift in laser frequency, and therefore is out of phase with the modulation frequency.

4 Performance of the Optical Phase Lock Loop

The direct carrier induced effect in contrast imposes a blue shift and is in phase with the modulation, but is weaker than the thermal contribution for small frequencies. For increasing modulation frequencies the temperature effect will fade out since the temperature can not follow the quick changes and the carrier effect will start to dominate. This crossing will result in a characteristic phase reversal of -180° in the modulation response of the complete response function of the diode [26, 27].

4.3.2 Performance of the Phase Lead-Lag Filter

The transfer function of the low pass and the lead lag filter was measured by simply adding the filter into circuit for the FM_{Laser} measurement. The lowpass has a cut-off frequency of 4.8 MHz. The lead-lag filter is mainly a high-pass with the cut-off frequency adjusted to a frequency in the interesting range for the bandwidth of the lock between 1 MHz and 2 MHz. The high pass will lift the phase and the low pass will lower the phase. This is the origin of the name lead lag filter. The measured curve is the red one in figure 4.7. It can be seen that the phase in the region from 100 kHz to around 1.5 MHz is lifted by 45° and with this increases the bandwidth of the loop. In the interesting region the phase for the feedback is lifted, while in uninteresting regions above the bandwidth the phase is worse than without the filter. To complete the analysis the finite time for the signal to go through the system has to be taken into account and the influence of the cavity has to be modeled. This is done in the next section.

4.3.3 The Finite Loop Delay

The propagation speed of a signal for the BNC cables is estimated to be $2/3$ of speed of light. For a cable length of 1.5 meters and an optical path of 1.25 m this results in a delay of 14 ns. For electronic components I will take the value estimated by [6] of 16 ns. This results in a total loop delay of $\tau = 30$ ns. The additional phase delay was calculated by

$$\phi_{\text{delay}} = -2\pi\nu\tau, \quad (4.14)$$

and added numerically to the measurement of the modulation response including the lead-lag filter (blue). The influence of the cavity can as well be modeled via equation 4.13 and leads to phase including all effects (green). The frequency where the phase delay is -90° can now be extracted from the graph to ≈ 2.5 MHz. The bandwidth is therefore slightly higher than the measured bandwidth extracted from the beat signal spectrum. The servo bumps there were in the region of 2 MHz, but after all, the contributions to the finite bandwidth are clear. The frequency modulation response of the laser itself seems to be the strongest limitation to the bandwidth of the loop and with that the broadening of the phase noise.

4.4 Conclusion

The measurements show that there are two possible ways for improving the setup. It might be possible to find a laser that provides a better reference. This would lead to

more power in the carrier, without the need to improve the bandwidth of the lock. The second possibility would be to shorten the length of the feedback loop, which might give a few nanoseconds, resulting in larger bandwidth, and with that possible more power in the carrier. The thermal response of the laser diodes however seems to be a serious constraint. The problem with the possible electronic noise of the PDF can be overcome in an elegant way presented in [28]. Here a small range in the linear response of the PFD around the origin is replaced is suppressed, and replaced by a classical mixer, that has less electronic noise. Another possibility to increase the performance of the lock would be to use lasers with an inherently smaller linewidth. The bandwidth of the lock would not need to be as high as for the laser diodes in order to lock the two lasers. On addition they also might show a different response to frequency modulation.

5 Electromagnetically Induced Transparency of a Single Atom

In the second chapter the functionality of the Raman setup was demonstrated. It is now set to be combined with the cavity, in order to exploit its full capabilities. As a first interesting result it was possible to demonstrate the effect of electromagnetically induced transparency (EIT) for a single atom. In order to do so the atoms are moved between the cavity mirrors via the optical conveyor belt. By the dispersive and absorptive interaction with the cavity mode, the transmission of the probe light through the cavity is changed with respect to the empty cavity without an atom inside. The Raman setup can then be used to phase lock the slave laser to the beam that is probing the cavity and with that as well to the cavity mode. By tuning the slave laser frequency it is then possible to control the interaction of the atom with the cavity mode. It is possible to switch the interaction of the atom with the cavity mode between absorptive and dispersive. The atom can even be rendered transparent for the cavity mode, hence the name EIT. Only by the strong enhancement of the interaction between probe beam and atom, due to the high reflectivity of the mirrors, it is possible to see the change in the refractive index, that is induced by the slave laser, for an single atom. In the first part of the chapter I will introduce the theoretical concept behind EIT. The presentation of the measurement and a first interpretation in a semi-classical picture follow.

5.1 EIT

The essence of EIT is to change the refractive index of an optical dense medium by coherently manipulating its internal energy states. A destructive interference between internal excitation channels on a two-photon resonance is the cause for the induced transparency. The most prominent case for this effect to appear is a medium consisting of atoms with a lambda-type energy level structure. The corresponding level scheme for a cesium atom is shown in figure 5.1. The atoms are coherently driven by a so called control laser, in the figure resonant with the $|1\rangle$ to $|3\rangle$ transition, and at the same time a probe laser, resonant with the $|2\rangle$ to $|3\rangle$ transition. The detuning of both lasers from the atomic resonance and the two-photon detuning between the two laser frequencies are as well depicted in the figure. In the experiment the probe beam will be very weak compared to the control beam, and in this limit the occurrence of EIT can be understood from the following argument:

The coupling of the strong control field results in a splitting of the atomic resonances, known as Autler-Townes splitting [29]. In figure 5.2 this splitting is illustrated for the case that both lasers are on resonance with their atomic transitions. In this case the splitting

5 Electromagnetically Induced Transparency of a Single Atom

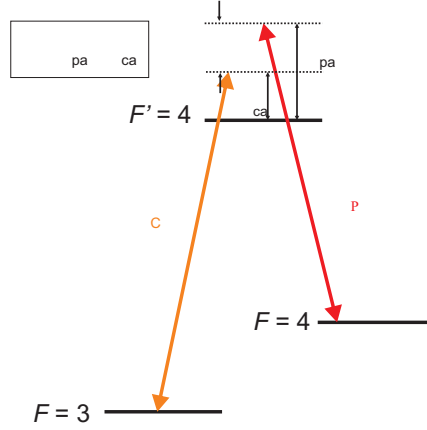


Figure 5.1: The lower ground state $F = 3$ ($|1\rangle$) is coupled via the control laser to the excited state $F' = 4$ ($|3\rangle$). The upper ground state $F = 4$ ($|2\rangle$) is coupled via the probe laser to the excited state. The two-photon detuning δ is chosen in such a way, that an increase in Δ_{CA} translates into a decrease in δ .

is symmetric. The two Autler-Townes levels are then split with an energy difference of Ω_{Control} . The two new Eigenstates can be expressed in the basis of the bare states of the atom $|1\rangle$ and $|3\rangle$ in the following way:

$$\begin{aligned} |a^+\rangle &= \frac{1}{\sqrt{2}}(|1\rangle + |3\rangle), \\ |a^-\rangle &= \frac{1}{\sqrt{2}}(|1\rangle - |3\rangle). \end{aligned} \quad (5.1)$$

In this limit of very weak probing the excitation from the $|2\rangle$ state can be seen as a spectroscopic measurement of the excited Autler-Townes states by the probe beam. Since it is unknown in which of the excited states the atom is, the modulus of the sum of possible excitation amplitudes has to be taken, exactly in the spirit of section 3.1. The dipole matrix element for the transition then reads

$$\begin{aligned} (\langle a^+| + \langle a^-|)d \cdot E_P |2\rangle &= \frac{1}{\sqrt{2}}(\langle 1| + \langle 3| + \langle 1| - \langle 3|)d \cdot E_P |2\rangle \\ &= \langle 1|d \cdot E_P |2\rangle = 0 \end{aligned} \quad (5.2)$$

The destructive interference between the excitation paths suppresses the absorption of both probe and control beam. The induced transparency gives rise to the name EIT for the effect.

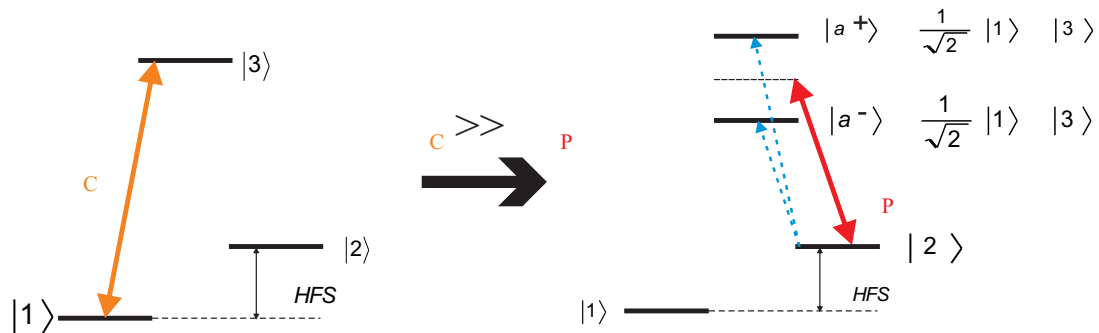


Figure 5.2: The strong coupling by a resonant control beam results in a symmetric splitting of the atomic resonance frequency. The two new created states are called Autler-Townes states. The excitation from the $|2\rangle$ state in the new states, can be seen as a spectroscopic measurement. When the probe beam is on resonance with its atomic transition the excitation will be suppressed by destructive interference between the two existing excitation channels.

For a more complete description of the situation the eigenstates of the lambda type level structure with possible detunings have to be taken into account. The Hamiltonian in the interaction picture for the three-level atom reads

$$H_{\text{Int}} = -\hbar \begin{pmatrix} \Delta_{CA} & 0 & -i\frac{\Omega_C}{2} \\ 0 & \Delta_{PA} & -i\frac{\Omega_P}{2} \\ i\frac{\Omega_C}{2} & i\frac{\Omega_P}{2} & 0 \end{pmatrix} \quad (5.3)$$

The energy zero point $E = 0$ is chosen to be the energy of the excited state $|3\rangle$. The coupling laser will shift the state $|1\rangle$ by Δ_{CA} from the zero point and the probe laser the state $|2\rangle$ by Δ_{PA} . The interaction between the levels is described by their coupling strengths on the off diagonal elements of the matrix. In principle this matrix can be diagonalized, but the analytic expression is rather uninformative and one has to rely on numerical solutions. For the case of a very weak probe beam however $\Omega_P \ll \Omega_C$, the off-diagonal element representing the interaction between probe beam and atom can be approximated to be zero. The new eigensystem then provides the energy of the two Autler-Townes states for all possible detunings of the control laser frequency from the atomic transition frequency

5 Electromagnetically Induced Transparency of a Single Atom

Δ_{CA} :

$$\begin{aligned} |a^+\rangle &= \sin(\phi) |1\rangle + \cos(\phi) |3\rangle \\ |a^-\rangle &= \cos(\phi) |1\rangle - \sin(\phi) |3\rangle \end{aligned} \quad (5.4)$$

with

$$\tan 2\phi = \frac{\Omega_C}{\Delta_{CA}} \quad \text{and} \quad E_{\pm} = \frac{\hbar}{2} \left(\Delta_{CA} \pm \sqrt{\Delta_{CA}^2 + \Omega_C^2} \right)$$

The excitation into these new formed dressed states from the $|2\rangle$ state will be suppressed on the two-photon resonance $\delta = 0$.

In order to calculate the full linear response of the system χ , also the time evolution of the states and a possible dephasing between the ground states has to be taken into account. The master equation for the limit of weak probing and including a possible dephasing between the ground states can be solved analytically to [30]:

$$\chi(\Delta_{PA}, \delta) = \frac{\mu_P^2 \rho}{\epsilon_0 \hbar} \left[-\frac{4\delta(|\Omega_C|^2 - 4\delta\Delta_{PA}) + 4\Delta_{PA}\gamma_{21}^2}{(|\Omega_C|^2 + (\gamma_{31} - i2\Delta_{PA})(\gamma_{21} - i2\delta))^2} \right. \quad (5.5)$$

$$\left. + i \frac{8\delta^2\gamma_{31} + 2\gamma_{21}(|\Omega_C|^2 + \gamma_{21}\gamma_{31})}{(|\Omega_C|^2 + (\gamma_{31} - i2\Delta_{PA})(\gamma_{21} - i2\delta))^2} \right], \quad (5.6)$$

where γ_{31} is the inverse decay time from $|3\rangle$ to $|1\rangle$ and γ_{21} models possible dephasing between the ground states $|2\rangle$ and $|1\rangle$. The amplitude depends on the density of the atoms ρ and the strength of the electronic dipole moment of the probe transition μ_P . The coupling strength would read $\Omega_P = \mu \cdot E_P/\hbar$. The model therefore does not include the intensity of the probe beam, since it was solved in the limit of very weak probing. I will summarize the amplitude under one single parameter

$$\alpha \equiv \frac{\mu_P^2 \rho}{\epsilon_0 \hbar} \quad (5.7)$$

With the knowledge about χ the response of an atom in free space is fully described.

5.2 Measurement

The important parameters for the experiment are the following: The resonance frequency of the cavity ω_r , which can be tuned via the length of the cavity. The frequency of the laser that is probing the cavity ω_P and its power P_P . And as well the frequency ω_C and power P_C of the control laser that illuminates the atoms from the open side of the cavity. The cavity resonance frequency is blue detuned from the atomic $F = 4$ to $F = 4'$ transition by 20 MHz and the probe laser is tuned in resonance with the empty cavity for all measurements. The reason for the detuning will now be explained. Due to the detuning between cavity

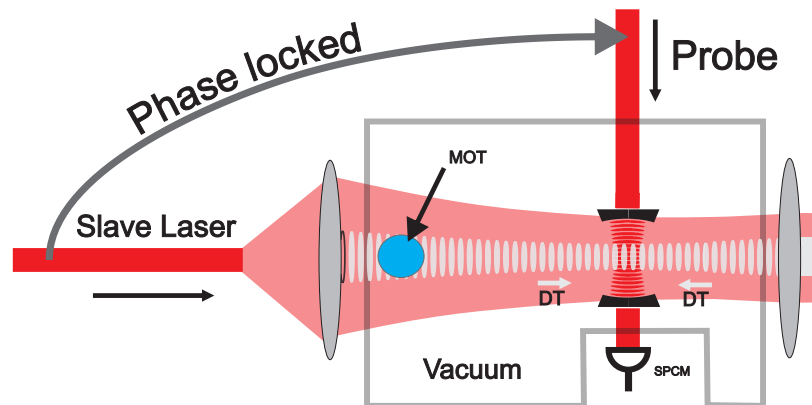


Figure 5.3: The atoms are moved via the optical conveyor belt inside the resonator. Probe laser and the slave laser are phase locked. The frequency of the slave laser is scanned over the two-photon resonance, while the transmission of the probe beam through the cavity is recorded with the single photon counting module (SPCM).

frequency and atomic transition, the atom interacts dispersively with the cavity mode, resulting in a frequency shift of the cavity resonance. The detuning of atom and cavity is now chosen in such a way that the transmission of the cavity with an atom inside will drop to around 50% of the empty cavity transmission. The resulting spectrum of the empty cavity resonance and the spectrum with a single atom placed inside the cavity are shown in figure 5.4. The plot is already done for the cavity parameters of our experiment, that will be given later. Also the way this spectrum is calculated is explained later in the interpretation section. For now it shall just illustrate the idea behind the measurement: Sitting on the steepest slope of the cavity resonance line makes the transmission sensitive to any additional change of χ induced by the interaction with the control field. A high contrast in the signal showing the EIT effect is expected. The power of the probe beam is so low, that on average only 0.1 photons are in the cavity mode. The slave laser of the Raman setup acts as the control laser and is phase locked to the probe laser of the cavity, see figure 5.3. The power in the beam is $1 \mu\text{W}$. The corresponding intensity at the position of the cavity could be calculated from the measured beam geometry in chapter 3. The resulting coupling strength Ω_C however will later be deduced from a fit, since this is more reliable. For the measurement the slave laser frequency is scanned over the two-photon resonance, while the transmission through the cavity is recorded with the single photon counting module. The sweeps are done in 10 ms for a two-photon-detuning from about -1 MHz to 1.5 MHz and then again in 10 ms from 1.5 MHz to -1 MHz. The average of such curves is taken. The short sweep time is necessary in order to minimize heating processes induced by the control laser during the frequency sweep. The heating would change the coupling between cavity mode and atom, which would result in an additional

5 Electromagnetically Induced Transparency of a Single Atom

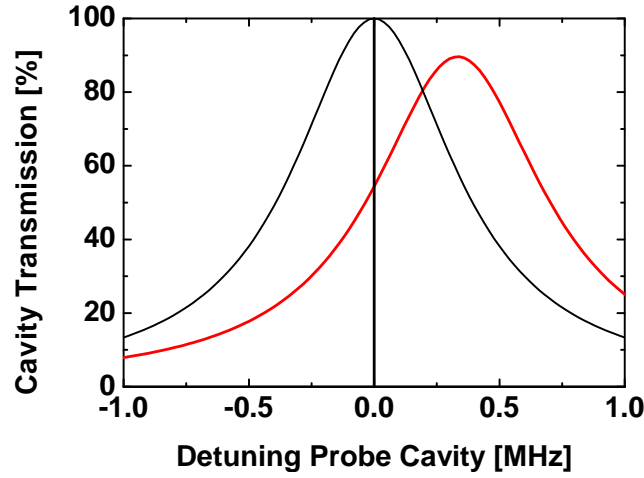


Figure 5.4: The black curve shows the resonance spectrum of an empty cavity. The red curve shows the shifted cavity resonance, when a single atom is placed inside the cavity. With the atom inside the cavity the transmission drops to around 50% of the empty cavity transmission. Sitting on the steep slope of the resonance line, makes the transmission sensitive to an additional change in the refractive index by the control beam.

change of transmission, whose origin is not the EIT effect and therefore should be avoided. The averaged transmission curves for 1 to 3 atoms for around 200 shots are shown in figure 5.5 and will now be interpreted in a semi-classical picture.

5.3 Interpretation of the Measurement

5.3.1 Semi-classical Approach

While the intensity of the coupling laser is large enough to treat the interaction with the atom as a strong perturbation, the situation for the probe beam is different. The cavity is probed so weakly that on average only 0.1 photons are inside the cavity. Due to the high reflectivity of the mirrors however the single photon would pass by the atom more than 300000 times before escaping through a cavity mirror. On its way the photon can accumulate the dispersive and absorptive interaction with the atom. Both can lead to change in the transmission of the probe beam through the cavity. When the photon is absorbed it will dominantly be scattered out to the side of the cavity. And thus the transmission would drop. The dispersive interaction will lead to new effective optical length of the cavity, which translates in a shift of the resonance frequency of the cavity. The probe light is not resonant anymore, which also results in a change in probe transmission through the cavity. Since the cross section for the the single interaction between the light passing the atom once is very small the EIT effect can be described in the limit of ($\Omega_C \gg \Omega_P$), where it can be seen as a splitting of the excited state by the coupling laser, and destructive

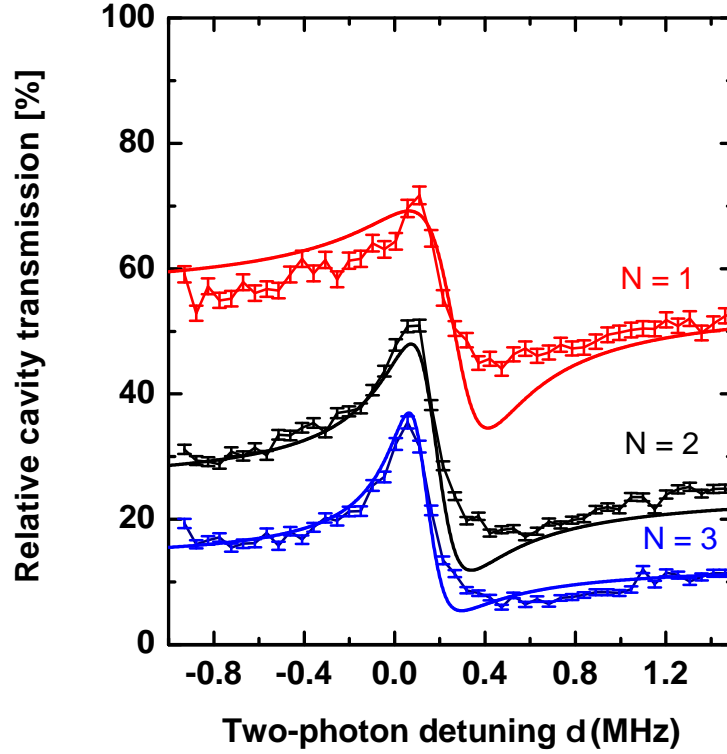


Figure 5.5: The averaged cavity transmission curves for over 200 sweeps of the slave laser frequency are shown for 1 to 3 atoms. The peak in transmission is identified with the EIT-resonance. The drop in transmission is identified with stronger absorption by the atoms inside the cavity. For the two-photon detuning the strong absorption occurs the cavity mode in resonance with an Autler-Townes level induced by the control beam. The EIT resonance is smeared out due to dephasing between the ground states of the atoms. The fit-curves of a semi-classical model are as well depicted in the plot.

interference suppressing the excitation by the probe beam.

The resulting Autler-Townes splitting for different detunings of control laser and atomic resonance frequency is drawn schematically in figure 5.6. The energy of the states can be calculated from equation 5.4. The coupling frequency is scanned over the two-photon resonance, resulting in different asymmetrical splittings of the dressed states. The dotted tilted line indicates the tuned frequency of the coupling beam. The probe frequency in contrast will stay fixed during the scan with a detuning of $\Delta_{PA}=20$ MHz and therefore its frequency is given as the horizontal dotted line in the figure. Two points in this figure should be highlighted. First when the detuning of coupling and atom is as well $\Delta_{CA} = 20$ MHz the two photon detuning is $\delta = 0$. This is the point A in the figure. The EIT effect occurs

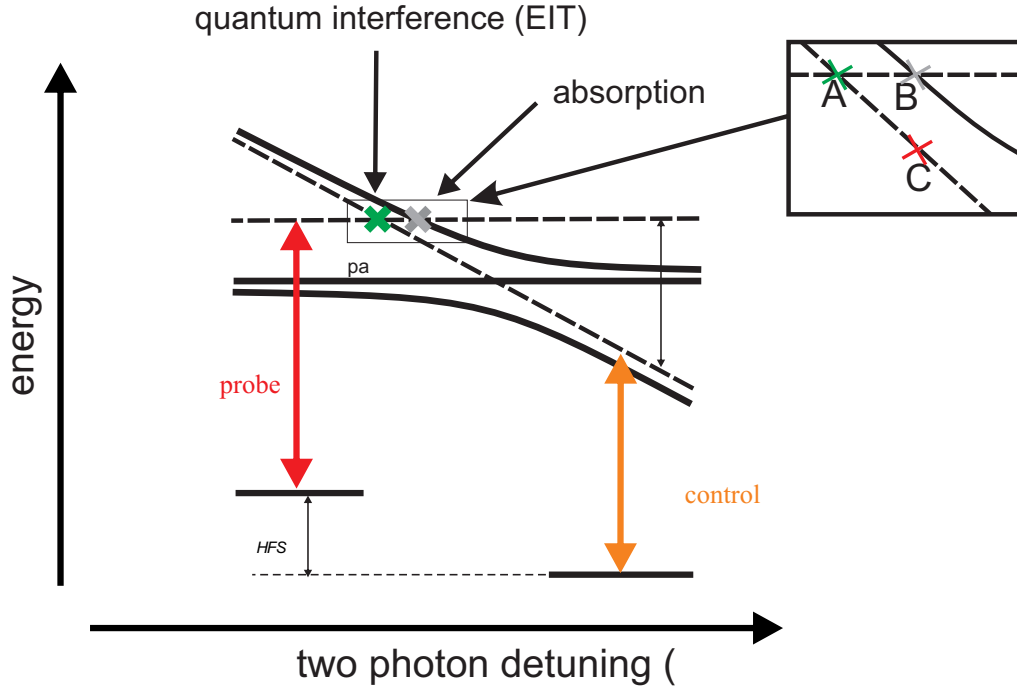


Figure 5.6: The strong coupling of the control beams splits the atomic $|2\rangle$ to $|3\rangle$ transition into the two Autler-Townes energy states. The probe beam stays at a fixed frequency with a detuning of Δ_{PA} . When the control frequency is scanned over the two-photon resonance two detunings should be emphasized. At point A the two-photon resonance occurs and the EIT effect appears. On point C the upper Autler-Townes level is in resonance with the probe beam, and strong absorption is expected.

and absorption and dispersion are zero.

The other important point is B: Here the upper dressed state is in resonance with the cavity probe beam and strong absorption is expected. An estimation for the detuning between these two points can be given from the following argument. For the large detuning of Δ_{PA} the energy of the probe beam and the upper dressed state are approximately parallel, and therefore the distances in between A and B is approximately the same as between B and C. The detuning difference between the EIT resonance and the strong absorption can therefore be calculated from the frequency difference between C and B using equation 5.4:

$$\delta_{\text{diff}} = \Delta_{PA} - \frac{4\Delta_{PA}^2 - \Omega_C}{4\Delta_{PA}^2} = \frac{\Omega_C^2}{4\Delta_{PA}} \quad (5.8)$$

The linear response χ can as well be calculated from 5.5 for the scan of the control laser frequency. Imaginary and real part of χ are plotted in figure 5.7. This is already done with a coupling strength of the control laser that will be later deduced from the fit to the

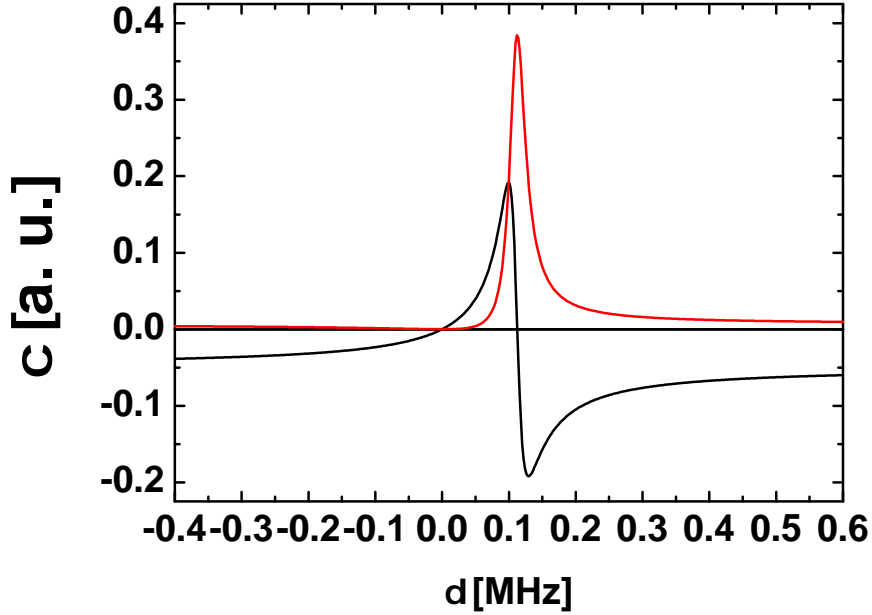


Figure 5.7: The expected linear response shows the EIT resonance at the two-photon resonance ($\delta = 0$), where absorption and dispersion are zero. The strong absorption corresponds to the probe beam resonance with the upper Autler-Townes energy level. This plot is not including any differential light shifts. Dephasing mechanisms are not included, too.

data. It reproduces the two points that were emphasized in the energy level scheme. On two-photon resonance ($\delta = 0$) absorption and dispersion are zero, the EIT effect occurs. For a detuning of around 0.1 MHz from the two-photon resonance the absorption peak corresponding to the upper dressed state can be seen. This is only the expected linear response of the atom in free space. The measurement however is done inside a cavity and the influence of χ on the cavity transmission has to be taken into account.

5.3.2 The Cavity

The cavity transmission is sensitive to both the dispersive and absorptive response of the atom. The transmission for of cavity is given by [14]

$$\frac{P_{\text{In}}}{P_{\text{Out}}} = \frac{T^2}{(T + A)^2 + 4(1 - T - A) \sin^2 \phi/2}. \quad (5.9)$$

Where R is the reflection, A the absorption and T the transmission of a single mirror forming a symmetric cavity. The phase ϕ is the round trip phase collected by the light. The influence of given χ on an assumed planar lighth wave reads for half the round trip

5 Electromagnetically Induced Transparency of a Single Atom

with ($|\chi| \ll 1$) reads

$$E_0 e^{-i(\omega t - nkr)} = E_0 e^{-i(\omega t - \sqrt{1+\chi}kr)} \approx e^{-i(\omega t - (1+\chi/2)kr)} \quad (5.10)$$

$$= e^{-i(\omega t - (1+\text{Re}(\chi)/2)kr)} e^{-(\text{Im}(\chi)/2)kr}. \quad (5.11)$$

The absorption of the light will be very small for a single round trip and can be modeled as an additional small absorption of the mirrors. Because the absorption A is related to the intensity the amplitude damping has to be squared. This results in

$$A' = A + (1 - e^{-k l \text{Im}(\chi)}) \approx A + k l \text{Im}(\chi) \quad (5.12)$$

where k is given by ω/c and l will be the interaction length of the light passing by the atom once, since the absorption is given for only one mirror. The round trip phase has the contribution of the light propagation itself and an additional dispersive effect arising from the interaction with the atom:

$$\phi = 2(kL + k l \text{Re}(\chi)/2) = 2\frac{\omega}{c}(L + l * \text{Re}(\chi)/2) \quad (5.13)$$

When the phase collected during the round trip is an integer multiple of 2π the constructive interference will result in maximal transmission. The cavity parameters were measured and can be found in [14]

$$A = 2.0 \cdot 10^{-6}, \quad T = 0.6 \cdot 10^{-6}, \quad L = 158 \mu\text{m} \quad (5.14)$$

[NOTE: The actual fitted model to the data differs by a factor of 2 in the relation between real and imaginary part of χ from the model presented here. A correction of the fit to the model, which is now believed to be correct, was not possible anymore due to time constraints.] The cavity transmission can now be calculated for a given χ . In theory the cavity transmission should always reach the empty cavity transmission on two-photon resonance, since there dispersion and absorption are zero. The smeared out line shapes in the measurement are due to the dephasing between the ground states. The amplitude α of χ depends on the density of atoms and the electronic dipole. Together with the interaction length the product αl will be a free fit parameter called the interaction strength. To summarize, it is now possible to fit a curve to the measured data with the three fit parameters: Ω_C the coupling strength between control beam, the strength of the interaction αl and the dephasing between the ground states γ_{21} .

The reasons for the dephasing are possible fluctuations in the magnetic field, fluctuating differential light shifts arising from power instabilities in the dipole trap and as well differential light shifts induced by the control beam. The scattering from dipole trap photons can be neglected. As already said, the semi-classical model presented in the limit of weak probing neglects the intensity of the probe beam. The high reflectivity of the mirrors in contrast strongly enhances the intensity inside the cavity. The semi-classical model fails to describe this. In order to make the model more realistic a heuristic approach can be made: A possible differential light shift δ_{LS} proportional to the intensity of the probe in the cavity

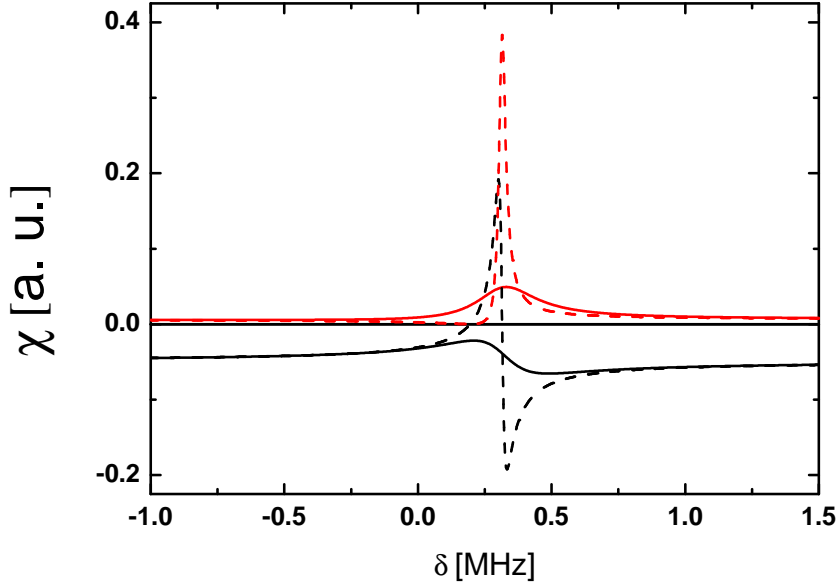


Figure 5.8: The red curves show the absorption of the single atom. The black curves show the dispersion of the single atom. The dotted lines are without dephasing, the continuous with dephasing. All curves include a differential light shift, that is shifting the two-photon resonance.

is as well included in the model to fit the data. This will also result in a dependency of the dephasing γ_{12} on the probe intensity in the cavity, since fluctuations in the differential light shift would cause dephasing. This assumptions no results in the following constraints for the fit depending on the atom number: First the interaction strength should scale with the number of atoms, since it is just an increase in density of the atoms. Second, additional dephasing and an additional light shifts should scale with the intra cavity intensity. Since the atom number changes the interaction strength, the intracavity intensity also depends on the atom number. The dephasing and a possible differential light shift can therefore as well depend on the atom number. The transmission level for $\delta = 1.5 MHz$ is taken as an average value for the intensity corresponding to the atom number, again this is strong simplification in order to keep the model simple. A linear relation between this transmission level and the additional differential lighth shifts is assumed. With these settings it is possible to fit curves to the measured data by hand with the following results

N	Ω_C [MHz]	$l \cdot \alpha [\frac{m}{10^{-12}}]$	γ_{21} [MHz]	δ_{LS} [MHz]
1	3.1	3.01	0.24	0.195
2	3.1	6.02	0.125	0.18
3	3.1	9.03	0.09	0.15

5 Electromagnetically Induced Transparency of a Single Atom

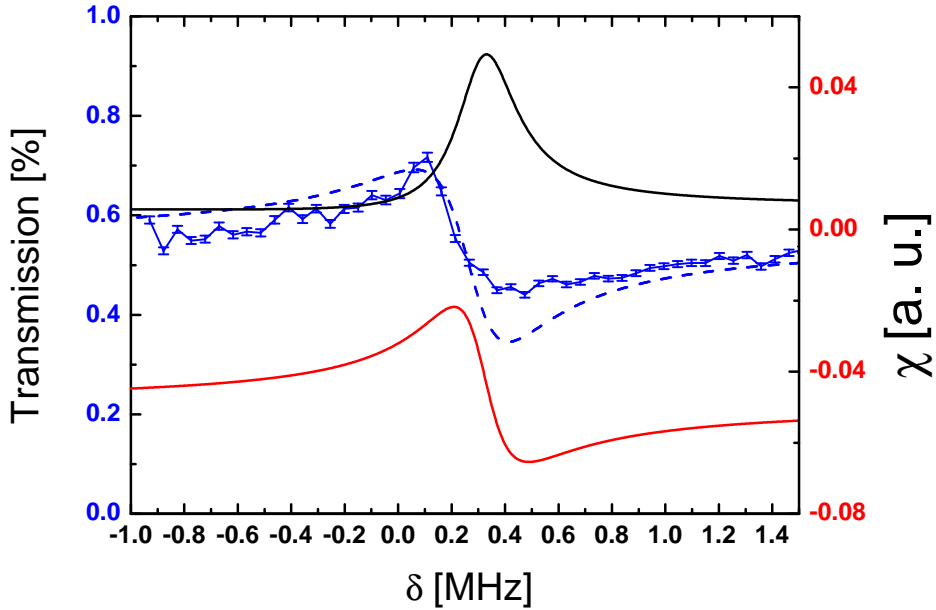


Figure 5.9: The measured cavity transmission for one atom with the fit curve is shown (blue). On addition the linear response with dephasing. The broadening of the absorption (red) pushes the point of maximal transmission to a smaller two-photon detuning. The maximal transmission appears at a detuning of $\delta=100$ kHz. The expected two-photon resonance including the differential light shift but without dephasing from the fit is however expected at a detuning of $\delta=200$ kHz, as it can be seen in figure 5.8. It therefore difficult to say for which exact detuning δ the EIT resonance occurs.

First it has to be noticed that the fit for one atom is the worst. In principle it is expected that the semi-classical approach works best for more atoms, since that is closer to our classical world. The fit was therefore done in order to get the best result for three atoms and then the fit for the other curves was extrapolated from this curve under the before mentioned constraints. The second important thing to notice is that the peak of maximum transmission does not belong to the expected EIT resonance without dephasing. In 5.8 χ is plotted for one atom with dephasing and without dephasing. From the plot it can be seen that the EIT resonance, shifted by the fitted differential light shift, should occur at a two-photon detuning of 200 kHz. The dephasing smears out the dispersive and absorptive contributions drastically. The dispersive response will always stay negative, in contrast to the theoretically expected changing of the sign around the EIT resonance. In plot 5.9 the measured curve for one atom, χ and the fitted curve are shown. The broadening of the absorption by the dephasing pushes the maximum transmission point to a smaller detuning, so that the maximal transmission occurs at a detuning of 0.1 kHz.

The dependence of the light-shift and dephasing on the intra cavity intensity are shown

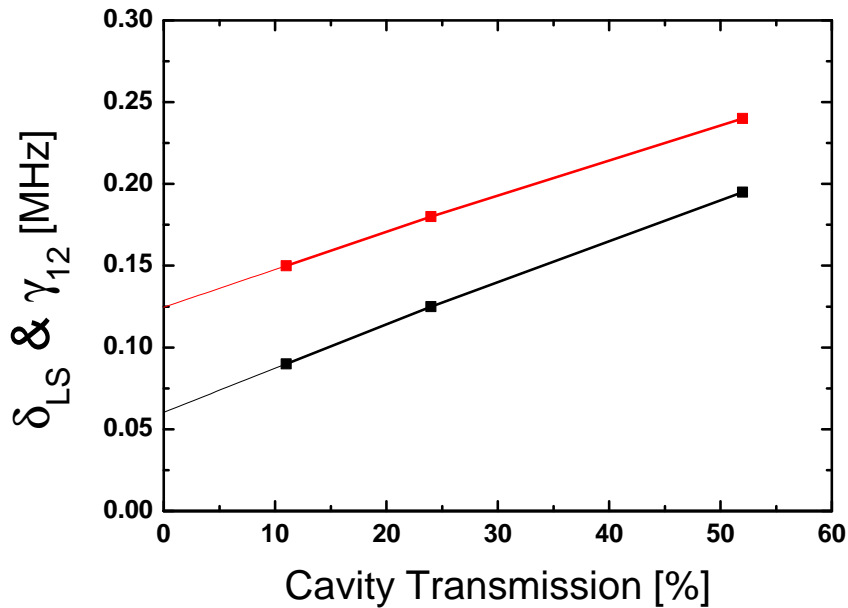


Figure 5.10: Dephasing γ_{12} (red curve) and differential light shift δ_{LS} (black curve) are plotted as a function of the cavity transmission for a two-photon detuning of 1.5 MHz. The linear dependence that was a constraint to the model for the fit is illustrated. By extrapolating the lines to zero, the residual dephasing and differential line shift can be deduced.

in figure 5.10. Since it was a constraint that the dependence should be linear it is easy to extrapolate the linear relation to zero. This should give the residual light shift and dephasing that does not depend on the intra cavity intensity. Sources for that could be the dipole trap or a possible residual magnetic field. The results are: $\delta_{res}=0.12$ MHz and for $\gamma_{res}=0.06$ MHz. To conclude, the model seems to explain the data sufficiently enough to state that the shape of the measured curves arises from an EIT effect.

5.4 Conclusion

The measurements show that EIT occurs for a single atom. The semi-classical model that was used to describe the measured data, however seems to fail in explaining the complete system in the limit of weak probing. A complete quantum theory is necessary to really predict the depending of the light shift and dephasing on the intra cavity intensity. In order to understand the dynamics of the system better more data need to be taken in the future.

6 Summary and Outlook

Summary

In this thesis I have presented the successful integration of two optically phase locked diode lasers into the main experiment. The functionality of this so called Raman setup was demonstrated by driving stimulated Raman-Rabi oscillations between atomic hyperfine states where the atoms are trapped in the dipole trap in front of the cavity. The induced Rabi oscillations had a frequency of around 20 kHz and the damping could be reduced to a level which is of the same order of magnitude as Rabi oscillations driven by microwave transitions in our experiment. Since microwave transitions have proven to be a reliable tool in the experiment, the performance was declared sufficient in order to proceed with the main experiment.

The performance of the optical phase lock loop itself was the object of further investigations. By observing the quadrature of the beat signal a new analysis tool was implemented that gives reliable information about the lock performance. The limiting factors to the performance of the lock were as investigated with the result, that the thermal response of the laser diodes to frequency modulation is the strongest constraint to the performance of the lock.

By locking the slave laser of the Raman setup onto the laser that is populating the cavity mode it was possible to detect the effect of EIT. In this context the cavity worked as a detection tool that is sensitive to both absorption and dispersion of the medium inside the cavity. The influence of the EIT effect on real and imaginary parts of the refractive index of the single atom thus could be observed in the measurement.

Outlook

In the near future a more complete understanding of the EIT measurement is the main task in the experiment. The full quantum model of the internal dynamics has to be worked out in detail in order to describe all differential light shifts and possible dephasing mechanisms more correctly. Also the external dynamics of the atoms inside the cavity is strongly influenced by the control beam. We conclude this from a measurement of the lifetime of the atoms inside the dipole trap potential well. For two-photon detunings close to the two-photon resonance, a drastic increase of the lifetime was observed. This possible new cooling effect is difficult to be distinguished from other cooling mechanisms inside the cavity. Even without the understanding of the effect, it has been used to cool the atoms between measurement cycles in order to obtain a more stable coupling between atom and cavity, which is always desired. On the long term scale the Raman setup opens up possibilities for

6 Summary and Outlook

a variety of experiments. The next step towards the entanglement of the atoms would be to drive the so called cavity-Raman-Rabi transitions. The principle behind these transitions is exactly the same as for the stimulated Raman-Rabi transitions described in chapter 3, but there the Stokes beam would be replaced by the cavity mode. The experimental setting would be very similar to the EIT measurement, only the mutual detunings between atom, cavity and control beam would change. The performance of the Rabi oscillation however is unpredictable since the Rabi frequency needs to be faster than the photon decay rate out of the cavity. This would lead to a Raman-Rabi frequency in the MHz range, where the performance of the Raman setup is not sufficiently tested. The Raman setup can as well be used as a tool to coherently manipulate the hyperfine ground states of the atom inside the cavity, by shining in both the master and the slave laser from the side of the cavity. The same stimulated Raman transitions that were driven in the dipole trap at the position of the MOT can be driven inside the cavity. The cavity would not be far detuned from the atomic resonance as it would be the case for cavity-Raman transitions, and the hyperfine state of the atoms is measured non-destructively via the cavity transmission level. These experiments could lead to intriguing effects such as the Quantum Zeno Effect.

Bibliography

- [1] Peter W. Shor, *Polynomial time algorithms for prime factorization and discrete logarithms on a quantum computer*, SIAM J. Sci. Statist. Comput. **26**, 1484 (1997)
- [2] R. Ursin, F. Tiefenbacher, T. Schmitt-Manderbach, H. Weier, T. Scheidl, M. Lindenthal, B. Blauensteiner, T. Jennewein, J. Perdigues, P. Trojek, B. Omer, M. Furst, M. Meyenburg, J. Rarity, Z. Sodnik, C. Barbieri, H. Weinfurter, and A. Zeilinger, *Entanglement-based quantum communication over 144 km*, Nature Physics (2007)
- [3] Ferdinand Schmidt-Kaler, Hartmut Haffner, Mark Riebe, Stephan Gulde, Gavin P. T. Lancaster, Thomas Deuschle, Christoph Becher, Christian F. Roos, Jurgen Eschner, and Rainer Blatt, *Realization of the Cirac-Zoller controlled-NOT quantum gate*, Nature (2003)
- [4] M. Khudaverdyan, W. Alt, T. Kampschulte, S. Reick, A. Thobe, A. Widera, and D. Meschede, *Quantum Jumps and Spin Dynamics of Interacting Atoms in a Strongly Coupled Atom-Cavity System*, Phys. Rev. Lett. **103**, 123006 (2009)
- [5] L. You, X. X. Yi, and X. H. Su, *Quantum logic between atoms inside a high-Q optical cavity*, Phys. Rev. A **67**, 032308 (2003)
- [6] Karsten Schörner, *Ein phasenstabilisiertes Lasersystem für resonatorinduzierte Raman-Prozesse*, Master's thesis, University Of Bonn (2008)
- [7] S. E. Harris, J. E. Field, and A. Kasapi, *Dispersive properties of electromagnetically induced transparency*, Phys. Rev. A **46**, R29–R32 (1992)
- [8] Min Xiao, Yong-qing Li, Shao-zheng Jin, and Julio Gea-Banacloche, *Measurement of Dispersive Properties of Electromagnetically Induced Transparency in Rubidium Atoms*, Phys. Rev. Lett. **74**, 666–669 (1995)
- [9] O. Schmidt, R. Wynands, Z. Hussein, and D. Meschede, *Steep dispersion and group velocity below $c/3000$ in coherent population trapping*, Phys. Rev. A **53**, R27–R30 (1996)
- [10] M. Fleischhauer and M. D. Lukin, *Dark-State Polaritons in Electromagnetically Induced Transparency*, Phys. Rev. Lett. **84**, 5094–5097 (2000)
- [11] A. D. Boozer, A. Boca, R. Miller, T. E. Northup, and H. J. Kimble, *Reversible State Transfer between Light and a Single Trapped Atom*, Phys. Rev. Lett. **98**, 193601 (2007)

Bibliography

- [12] L.-M. Duan and H. J. Kimble, *Scalable Photonic Quantum Computation through Cavity-Assisted Interactions*, Phys. Rev. Lett. **92**, 127902 (2004)
- [13] Wolfgang Alt, *Optical control of single neutral atoms*, Ph.D. thesis, University of Bonn (2004)
- [14] Igor Dotsenko, *Single atoms on demand for cavity QED experiments*, Ph.D. thesis, University of Bonn (2007)
- [15] Stefan Kuhr, *A controlled quantum system of individual neutral atoms*, Ph.D. thesis, University of Bonn (2003)
- [16] B. W. Shore, *The Theory of Coherent Atomic Excitation, Volume 2, Multilevel Atoms and Incoherence* (1990)
- [17] James Bateman, Andre Xuereb, and Tim Freegarde, *Stimulated Raman transitions via multiple atomic levels*, arxiv.org (2009), URL <http://arxiv.org/abs/0908.2389>
- [18] Daniel Adam Stack, *Cesium D Line Data* (2009)
- [19] S. Kuhr, W. Alt, D. Schrader, I. Dotsenko, Y. Miroshnychenko, A. Rauschenbeutel, and D. Meschede, *Analysis of dephasing mechanisms in a standing-wave dipole trap*, Phys. Rev. A **72**, 023406 (2005)
- [20] Mkrtych Khudaverdyan, *A controlled one and two atom-cavity system*, Ph.D. thesis, Rheinischen Friedrich-Wilhelms-Universität Bonn (2009)
- [21] Norihito Kosugi, Shigemasa Matsuo, Kohkichi Konno, and Noriyuki Hatakenaka, *Theory of damped Rabi oscillations*, Phys. Rev. B **72**, 172509 (2005)
- [22] Miao Zhu and John L. Hall, *Stabilization of optical phase/frequency of a laser system: application to a commercial dye laser with an external stabilizer*, J. Opt. Soc. Am. B **10**, 802–816 (1993), URL <http://josab.osa.org/abstract.cfm?URI=josab-10-5-802>
- [23] Dennis W. Ricker, *Echo Signal Processing*, Kluwer Academic Publishers (2003)
- [24] Li Lu-Ming, Tang Wen-Zhuo², Hu Zhen-Yan², and Guo Hong², *Realization of Optical Phase Locked Loop at 9.2 GHz between Two Independent Diode Lasers*, Chinese Physics Letters (2008)
- [25] Prof Dr.-Ing. Jan Lunze, *Regelungstechnik*, Springer (2008)
- [26] P. Corrc, O. Girad, and I. F. de Faria, *On the thermal contribution to the FM response of DFB lasers: theory and experiment*, IEEE Journal of Quantum Electronics **30**, 2485–2490 (1994)

- [27] Wei Lang, *Study of Optical Phase Lock Loops and the Applications in Coherent Beam Combining and Coherence Cloning*, Ph.D. thesis, CALIFORNIA INSTITUTE OF TECHNOLOGY (2008)
- [28] L. Cacciapuoti, M. de Angelis, M. Fattori, G. Lamporessi, T. Petelski, M. Prevedelli, J. Stuhler, and G. M. Tino, *Analog + digital phase and frequency detector for phase locking of diode lasers*, Review of Scientific Instruments **76**, 053111 (2005), URL <http://link.aip.org/link/?RSI/76/053111/1>
- [29] Serge Haroche and Jean-Michel Raimond, *Exploring the Quantum*, Oxford Graduate Texts (2006)
- [30] Michael Fleischhauer, Atac Imamoglu, and Jonathan P. Marangos, *Electromagnetically induced transparency: Optics in coherent media*, Rev. Mod. Phys. **77**, 633–673 (2005)

Danksagung

Mein Dank gilt allen, die mich beim Erstellen dieser Arbeit unterstützt haben.

Zuallererst möchte ich mich bei Herrn Professor Meschede dafür bedanken, dass ich meine Diplomarbeit an diesem abwechslungsreichen und lehrreichen Experiment erstellen durfte. Mein weiterer Dank gilt Frau Priv.-Doz. Soergel für die Übernahme des Korreferats.

Ein besonderes Dankeschön gilt den Leuten mit denen ich zusammen im Labor gearbeitet habe. Insbesondere Tobias war während der gesamten Zeit ein geduldiger und hilfsbereiter Ansprechpartner. René und Stephan haben mir ebenfalls sehr geholfen. Allen drei möchte ich für die entspannte und motivierende Atmosphäre im Labor danken. Auch Sebastian und Lingbo, die die Gruppe bereits verlassen haben, standen mir am Anfang mit Rat und Tat zur Seite.

Den PostDocs Wolfgang und Artur danke ich für die vielfache Unterstützung bei den immer wieder auftauchenden physikalischen und technischen Problemen. Wolfgang hat nicht nur durch sein unerschöpfliches Wissen maßgeblich zur Arbeit beigetragen, sondern auch durch seine fortlaufende Versorgung mit Orangen, Schokolade und Tee für eine ausgewogene Ernährung während meiner Zeit in der Gruppe gesorgt.

Auch allen anderen Mitgliedern der Gruppe möchte ich danken für die Hilfe, die Unterstützung und die gute Zeit.

Meinen Eltern möchte ich danken, dass Sie mich immer unterstützen und mir die Möglichkeit gegeben haben ein Semester im Ausland zu studieren.

Erklärung

Ich versichere, dass ich diese Arbeit selbständig verfasst und keine anderen als die angegebenen Quellen und Hilfsmittel benutzt sowie die Zitate kenntlich gemacht habe.

Referent: Prof. Dr. Dieter Meschede
Koreferent: Priv.-Doz. Dr. Elisabeth Soergel